



Low- and intermediate-temperature ammonia/hydrogen oxidation in a flow reactor: Experiments and a wide-range kinetic modeling

Alessandro Stagni^{a,*}, Suphaporn Arunthanayothin^b, Mathilde Dehue^b, Olivier Herbinet^b,
Frédérique Battin-Leclerc^b, Pierre Bréquigny^c, Christine Mounaïm-Rousselle^c,
Tiziano Faravelli^a

^a Department of Chemistry, Materials, and Chemical Engineering "G. Natta", Politecnico di Milano, Milano 20133, Italy

^b Laboratoire Réactions et Génie des Procédés, CNRS-Université de Lorraine, 1 rue Grandville, 54000 Nancy, France

^c Université Orléans, INSA-CVL, EA 4229 – PRISME, F-45072 Orléans, France

ARTICLE INFO

Keywords:

Ammonia
Hydrogen
Flow reactor
Nitrogen oxides
Detailed kinetics

ABSTRACT

Understanding the chemistry behind the oxidation of ammonia/hydrogen mixtures is crucial for ensuring the flexible use of such mixtures in several applications, related to propulsion systems and power generation. In this work, the oxidation of ammonia/hydrogen blends was investigated through an experimental and kinetic-modeling study, where the low- and intermediate-temperature conditions were considered. An experimental campaign was performed in a flow reactor, at stoichiometric conditions and near-atmospheric pressure (126.7 kPa). The mole fraction of fuels, oxidizer and final products was measured. At the same time, a comprehensive kinetic model was set up, following a modular and hierarchical approach, and implementing the recently-available elementary rates. Such a model was used to interpret the experimental results, and to extend the analysis to literature data, covering several oxidation features. The reactivity boost provided by H₂ addition was found to be approximately linear with its mole fraction in both flow- and jet-stirred-reactor conditions (except for the smallest H₂ amounts in the flow reactor), in contrast with the more-than-linear increase in the laminar flame speed. The key role of HO₂ in regulating fuel conversion and autoignition at low temperature was confirmed for binary mixtures, with H₂NO being the bottleneck to the low-temperature oxidation of NH₃-rich blends. On the other hand, the nitrogen fate was found to be mostly regulated by NH_x + NO propagation and termination channels.

1. Introduction

As the energy infrastructure is being fed by increasing quotas of renewable sources, ensuring a continuous energy supply starting from intrinsically discontinuous sources, e.g. sun, wind or waves, has become a topical issue in the current energy transition. Reformulating the concept of energy storage is then a mandatory step to enable such a switch, and for this reason energy research has recently put the spotlight on chemical energy carriers [1–3] to fulfill this task. Yet, in this scenario, one major constraint needs to be accounted for, i.e. achieving an energy system as much as possibly CO₂-neutral, such to meet the reduction targets of greenhouse gases (GHGs) [4].

The most immediate way to implement a CO₂-neutral energy infrastructure is the introduction of carbon-free fuels, and the two most appealing candidates in this direction have been hydrogen (H₂) [5,6]

and, more recently, ammonia (NH₃) [3,7,8]. Concerning the former, the development of a hydrogen-based economy has been envisioned for decades, but is still struggling with several techno-economical challenges, among which production, storage, distribution and safety are worth being mentioned [5,9]. On the other hand, ammonia has become more and more attractive in the latest years, to the extent that an NH₃ [10] or an NH₃/H₂ [11] economy have been theorized.

As a matter of fact, the physico-chemical properties of NH₃ ease many of the transportation and storage issues faced by hydrogen, since at ambient temperatures it can be liquefied at much lower pressures (~8 bar instead of ~700 bar). Moreover, due to its historical central role in the chemical industry, its production technologies are well established [12], and its uses are countless, including fertilizers, explosives, household products, and a variety of other chemicals. Due to such a multiplicity of applications, the distribution network is quite consolidated, occurring via pipelines, shipping or trucks [13].

* Corresponding author.

E-mail address: alessandro.stagni@polimi.it (A. Stagni).

<https://doi.org/10.1016/j.cej.2023.144577>

Received 28 February 2023; Received in revised form 9 June 2023; Accepted 1 July 2023

Available online 3 July 2023

1385-8947/© 2023 The Author(s). Published by Elsevier B.V. This is an open access article under the CC BY license (<http://creativecommons.org/licenses/by/4.0/>).

Nomenclature

Roman symbols

P	Pressure [Pa]
T	Temperature [K]
X	Mole fraction [-]

Greek symbols

η	Yield [-]
τ	Residence time [s]
Φ	Equivalence ratio [-]

Acronyms

CFD	Computational Fluid Dynamic
FR	Flow Reactor
GHG	Greenhouse Gas
IDT	Ignition Delay Time
LFS	Laminar Flame Speed
MILD	Moderate or Intense Low-Oxygen Dilution
NO _x	Nitrogen Oxides (NO, NO ₂ , N ₂ O)
PFR	Plug Flow Reactor
RCM	Rapid Compression Machine
ROPA	Rate of Production Analysis
ST	Shock tube

Subscripts

c	Compression
u	Unburned gas

On the other hand, the biggest drawbacks limiting a massive use of NH₃ as fuel are of chemical nature, since it exhibits both an extremely low burning velocity and a high resistance to auto-ignition, when compared to hydrogen as well as other conventional fuels [14]. In addition, the presence of nitrogen in the fuel molecule adds the further complication of Nitrogen Oxides (NO_x) formation through the fuel-NO_x pathway [15], whose contribution sums up to the usual thermal route [16]. NO_x include NO and NO₂, harmful for both environment (acid rains) and human health (asthma, dyspnea, etc.) as well as N₂O, among the most powerful GHGs, with a radiative forcing factor of ~300 times higher than CO₂ [17]. As a result, a comprehensive understanding of ammonia combustion kinetics is still needed, especially concerning the low-temperature conditions and high oxygen concentrations [15]. Anyway, in the latest years significant steps forward have been taken in this direction [18–20], mainly thanks to the advances in theoretical chemistry [21,22].

To address these issues while still keeping the benefits of ammonia as an energy vector, the most immediate solution is represented by blended mixtures, since conventional, more reactive fuels like methane, heavier hydrocarbons and hydrogen can be added to ammonia itself to compensate for its lack of reactivity, and to create tailor-made fuel mixtures with the desired reactivity features. In particular, the coupling between NH₃ and H₂ has recently raised the biggest interest in this area, and for several reasons: i) like ammonia, hydrogen is carbon-free; ii) significant research has been performed on hydrogen as a fuel and an energy carrier in the latest decades; iii) hydrogen can be directly obtained from the upstream catalytic decomposition of NH₃ through a variety of catalysts [23]; iv) hydrogen can enhance the flame propagation features of NH₃ and improve its flame stability due to the larger range of flammability limits. As a result, plenty of techno-economical analyses on ammonia-hydrogen fueled systems have been performed in the recent past, for both internal combustion engine [24–28] and gas turbine [29,30] applications.

In addition, the research on combustion devices fed by NH₃/H₂ mixtures intersects with the increasing trend of exploration of novel

combustion concepts and regimes, in less conventional conditions (e.g. lower temperatures and/or high dilution levels), able to ensure a significant reduction of pollutant emissions while keeping high efficiency levels: flameless [31,32] and Moderate or Intense Low Oxygen Dilution (MILD) [33] regimes are among the most representative examples. Under these conditions, lower temperatures result in lower reaction rates, thus the whole combustion process is kinetically controlled, and an accurate description of chemistry is needed. While hydrogen kinetics is well-established in all of its elementary reaction rates [34,35], the oxidation of ammonia is still far from being fully understood. In their review on nitrogen chemistry, Glarborg et al. [15] highlighted the need for further investigation of low-temperature, oxygen-rich conditions for ammonia combustion, at both an experimental and a theoretical level. This is true for NH₃/H₂ mixtures, too, for which an increasing number of experimental campaigns have been recently performed at several institutions. In parallel to the study of NH₃ as a pure fuel [20,36–42], research has intensified on NH₃/H₂ blends. High-temperature ignition delay times (IDT) of pure NH₃ and H₂ fuels and related mixtures were recently measured in a shock tube (ST) by Chen et al. [43] and Alturaifi et al. [44], while low-temperature ignition delay times were obtained by Pochet et al. [45], Dai et al. [46] and He et al. [47] in Rapid Compression Machines (RCM). The results of these latter studies were particularly interesting, since they highlighted a non-linear dependence of ignition delay time on the amount of added hydrogen. In addition, Jet-Stirred Reactors (JSR) were used in several studies to obtain an insight on low-temperature reactivity and species formation [48,49]. The availability of speciation data is of critical importance for kinetic model development, since the selectivity in nitrogen-containing compounds is a key parameter to be reproduced, in order to assess the pollution potential of NH₃/H₂ blends. In the same devices, dynamic regimes (e.g. oscillations), were also identified [50], which are also a critical benchmark for mechanism validation, since they involve the overlapping of chemistry, mass flow and heat exchange phenomena [51]. In terms of flame propagation features, plenty of datasets on laminar flame speeds (LFS) on such mixtures have been made available in the last decade [52–58]. All of them pointed out a more-than-linear increase of the burning velocity with the hydrogen mole fraction.

At a theoretical level, the knowledge on ammonia pyrolysis and oxidation mechanism has recently expanded thanks to an extensive use of quantum-chemistry based tools [22,59,60] for an accurate and relatively quick estimation of the critical rate constants affecting ammonia combustion. These were then implemented in the most recent kinetic mechanisms describing ammonia oxidation [15,20,38,47,61–63]. Due to the hierarchy principle, all of these mechanisms are suited to describe the oxidation of NH₃/H₂ mixtures, too, and can then be used to interpret the interaction between the two fuels in triggering both ignition and flame propagation.

In order to ascertain the combustion features of NH₃/H₂ mixtures and the mutual interaction between the two fuels, this work aims at investigating the oxidation of such blends in the low- and intermediate-temperature regime, and diluted conditions, barely explored to date, in terms of both reactivity and pollutants emissions. To this purpose, an experimental campaign was carried out in a flow reactor (FR) by considering the oxidation of fuel mixtures with variable molar ratios between the two fuels. To the authors' knowledge, no parametric study of this kind has been performed so far in such an ideal facility. Lean conditions were chosen as they were shown to be particularly challenging and uncertain from a kinetic point of view [15]. On these premises, an established kinetic mechanism describing the pyrolysis and oxidation of ammonia was revised and exploited to interpret the obtained results, and to explain the reactivity triggers as well as the kinetic competitions driving nitrogen selectivity. Finally, the mechanism was applied to the wider range of literature experimental data obtained in several configurations (RCM, JSR, laminar premixed flames), and the controlling pathways were identified and compared to what is obtained in the adopted experimental configuration. Further validation of the

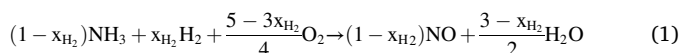
mechanism against the remaining experimental datasets is available as Supplemental Material (SM) of this work.

2. Methodology

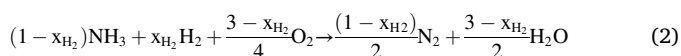
Hereafter, the experimental method and the formulation of the kinetic model are described, as well as the numerical tools adopted.

2.1. Experimental setup

The oxidation of ammonia/hydrogen mixtures was experimentally investigated using a tubular flow reactor located in an oven. This setup was previously used for the study of the oxidation of neat ammonia [20] and ammonia-methane mixtures [64]. Its outlet pressure was set to 950 torr (126.7 kPa). The consumption of the two co-fuels, ammonia and hydrogen, and the mole fraction of products were measured as a function of the reaction temperature for 6 mixtures composed of 1000 ppm of ammonia and of variable amounts of hydrogen over the range 0–2000 ppm (Table 1). A seventh mixture containing only 1000 ppm hydrogen was also considered as a reference. The equivalence ratio Φ_{NO} is always equal to 1, calculated according to the global reaction:



where x_{H_2} is the fraction of hydrogen in the fuel (mol/mol): $x_{H_2} = \frac{x_{H_2}}{x_{H_2} + x_{NH_3}}$, and NH_3 conversion to NO and H_2O is considered. However, it is worth noticing that this is not the only definition commonly adopted in literature to evaluate the equivalence ratio Φ . As will be presented in Section 3, several works consider N_2 as the ultimate oxidation product of NH_3 , and Φ_{N_2} results from the following reaction:



This is adopted, too, for mechanism validation purposes.

Inlet flows were adjusted for each investigated temperature in order to keep the residence time constant in the central part of the tube, where the temperature is quasi constant (measured profiles are provided in SM). The residence time in the central part is thus about 50 ms. Inlet flows were controlled using mass flow controllers provided by Bronkhorst (relative uncertainty in flow of 0.5%). Helium and hydrogen were provided by Messer (purity of 99.999%). The ammonia/helium mixture (2004 ± 60 ppm) used for experiments was also provided by Messer.

Species were sampled at the outlet of the reactor and analyzed online using mass spectrometry and a dedicated analyzer for NO_x . For the first diagnostic, the sampling was achieved thanks to a stainless-steel capillary tube connected to a quadrupole mass spectrometer (Omnistar from Pfeiffer) with ionization by electron impact at 70 eV. It was used for the detection of ammonia, hydrogen, oxygen, water, nitrogen, and NO . The calibration was performed by injecting standards except for water, which was calibrated considering the combustion as complete at the highest temperatures. The second diagnostic was a dual-channel NO_x analyzer (Thermo Scientific Model 42i), also used for the detection of NO_2 (confirming that no NO_2 was observed under the conditions of this study). The NO_x analyzer is equipped with an ammonia trap, to avoid

interferences due to the possible detection of this species. The relative uncertainty in mole fractions was ± 10% for all species. H-, O- and N-atom balances have been calculated for all experiments and are 0.97 ± 0.02 regardless of the atom (data are available in SM).

2.2. Kinetic model

The kinetic model describing NH_3/H_2 pyrolysis and oxidation was built starting from the previous work by Stagni et al. [20], and Table 2 lists the most relevant reactions, either updated or relevant for the different kinetic analyses (Section 3). In the mentioned work, the mechanism was developed following a first-principles approach: by combining sensitivity analysis of NH_3 conversion in the investigated conditions with a literature review of the uncertainty range of the critical reactions identified, a specific set of reactions was theoretically investigated, i.e. ammonia (R1) and HNO (R9) decompositions (pressure-dependent) along with H-abstractions by the main radicals (R3 to R6). The adopted methodology was the *ab initio* transition state theory based master equation (ME) approach (AITSTME) implemented into the EStokTP software [22]. Following a hierarchical and modular approach, the NH_3 sub-mechanism was added on top of a core H_2/O_2 mechanism, taken from the established work of Metcalfe et al. [35], and subset of NO_x reactions adopted after the work of Song et al. [65].

The mechanism was further improved via the update of specific sub-mechanisms, on the basis of the recently available theoretical calculations, as well as previous uncertainty and sensitivity analysis. The N_xH_y reaction mechanism was revised, following the latest theoretical findings: specifically, H-abstractions from NH_2 and N_2H_2 were adopted after the comprehensive study by Li and Sarathy [66] (R20 to R23), while NH/NH_2 mutual interactions were updated according to the theoretical work of Klippenstein et al. [67] (R25 to R31). The propagation and termination channels of the $NH + NO$ reaction, providing $N_2O + H$ and $N_2 + OH$, respectively, were updated by considering the overall rate and branching ratios recommended by Baulch et al. [68] (R34 and R35). Finally, a further update involved the thermal NO_x model, by introducing the recommended rate by Abián et al. [16] for R38.

The final mechanism, accounting for 31 species and 203 reactions, was successfully validated against a wide range of experimental data on NH_3 pyrolysis and oxidation, and is attached (in CHEMKIN format) in the SM. The validation of this model was not limited to the datasets obtained in the dedicated experimental campaign, but also included i) ignition delay times in shock tubes and RCMS, ii) speciation in jet stirred reactors, flow reactors and burner-stabilized flames, and iii) laminar flame speeds. Details are provided in the SM of the reference work [20].

2.3. Numerical tools

The numerical simulations were performed via the OpenSMOKE++ suite of solvers for ideal reactors [81], developed at Politecnico di Milano with the purpose of simulating reacting systems with detailed kinetic mechanisms. Flow reactor simulations were performed by considering perfect segregation, i.e. a Plug Flow Reactor (PFR) model, with an imposed temperature profile as recorded from thermocouple measurements for the different nominal temperatures. RCMS were

Table 1
Summary of the experimental conditions investigated in this study.

Set ID	$X_{NH_3}^{inlet}$ (ppm)	$X_{H_2}^{inlet}$ (ppm)	$X_{O_2}^{inlet}$ (ppm)	Mixture composition ($NH_3 : H_2$)	Φ_{NO} (1)	Φ_{N_2} (2)
1		0	1250	100.0:0.0		0.600
2		111	1306	90.0:10.0		0.617
3		266	1383	79.0:21.0		0.638
4	1000	538	1519	65.0:35.0	1.000	0.671
5		1000	1750	50.0:50.0		0.714
6		2003	2250	33.3:66.7		0.778
7	0	1000	500	0:100		1.000

Table 2

Most relevant reactions in the NH₃/H₂ oxidation sub-mechanism. Reaction rate expression is modified Arrhenius $k = AT^{\beta}\exp[-E_{\text{act}}/(RT)]$. Units are cm³, cal, mol, K. CHEMKIN keywords are adopted.

ID	Reaction	A	β	E _{act}	Notes	Ref
R1	NH ₃ = NH ₂ + H	7.230 × 10 ²⁹	-5.316	110862.4	0.1 atm	[20]
		3.497 × 10 ³⁰	-5.224	111163.3	1 atm	
		1.975 × 10 ³¹	-5.155	111887.8	10 atm	
		2.689 × 10 ³¹	-4.920	112778.7	100 atm	
R2	NH ₃ + H = NH ₂ + H ₂	1.963 × 10 ⁴	2.854	8520.2		[20]
R3	NH ₃ + OH = NH ₂ + H ₂ O	1.559 × 10 ⁵	2.372	118.9		[20]
R4	NH ₃ + O = NH ₂ + OH	4.430 × 10 ²	3.180	6739.9		[20]
R5	NH ₃ + O ₂ = NH ₂ + HO ₂	1.415 × 10 ¹⁰	1.285	55224.0		[20]
R6	NH ₃ + HO ₂ = NH ₂ + H ₂ O ₂	1.173 × 10 ⁰	3.839	17260.0		[20]
R7	NH ₂ + HO ₂ = H ₂ NO + OH	1.566 × 10 ¹³	0.000	0.0		[68]
R8	NH ₂ + HO ₂ = HNO + H ₂ O	2.190 × 10 ⁹	0.791	-1428.0		[60]
R9	HNO = H + NO	2.104 × 10 ²⁰	-3.151	48651.0	0.1 atm	[20]
		1.568 × 10 ²¹	-3.113	48707.0	1 atm	
		1.060 × 10 ²²	-3.059	48978.0	10 atm	
		4.976 × 10 ²²	-2.963	49471.0	100 atm	
R10	NO + HO ₂ = NO ₂ + OH	2.110 × 10 ¹²	0.000	-480.0		[69]
R11	NH ₂ + NO = NNH + OH	4.300 × 10 ¹⁰	0.294	-866.0		[70]
R12	NH ₂ + NO = N ₂ + H ₂ O	2.600 × 10 ¹⁹	-2.369	870.0		[70]
R13	NH ₂ + NO ₂ = H ₂ NO + NO	8.600 × 10 ¹¹	0.110	-1186.0		[15]
R14	NH ₂ + NO ₂ = N ₂ O + H ₂ O	2.200 × 10 ¹¹	0.110	-1186.0		[15]
R15	H ₂ NO + O ₂ = HNO + HO ₂	2.300 × 10 ²	2.994	16500.0		[15]
R16	H ₂ NO + NO ₂ = HNO + HONO	6.000 × 10 ¹¹	0.000	2000.0		[71]
R17	H ₂ NO + NH ₂ = HNO + NH ₃	1.800 × 10 ⁶	1.940	-1152.0		[72]
R18	H ₂ NO + HO ₂ = HNO + H ₂ O ₂	3.360 × 10 ⁵	2.000	-1434.0		[20]
R19	H ₂ NO + OH = HNO + H ₂ O	2.400 × 10 ⁶	2.000	1192.2		[72]
R20	N ₂ H ₂ + H = NNH + H ₂	4.820 × 10 ⁸	1.760	739.0		[66]
R21	N ₂ H ₂ + O = NNH + OH	1.110 × 10 ⁸	1.620	805.0		[66]
R22	NH ₂ + H = NH + H ₂	1.090 × 10 ⁵	2.590	1812.0		[66]
R23	NH ₂ + OH = NH + H ₂ O	4.040 × 10 ⁴	2.520	-616.0		[66]
R24	NH ₂ + O = HNO + H	1.500 × 10 ¹⁵	-0.547	836.7		[73]
R25	DUPLICATE	7.730 × 10 ¹³	-0.277	646.4		[73]
	NH ₂ + NH ₂ = N ₂ H ₂ + H ₂	1.700 × 10 ⁸	1.620	11783.0		[67]
R26	NH ₂ + NH ₂ = H ₂ NN + H ₂	7.200 × 10 ⁴	1.880	8802.0		[67]
R27	NH ₂ + NH ₂ = NH ₃ + NH	5.640 × 10 ⁰	3.530	550.0		[67]
R28	NH ₂ + NH ₂ (+M) = N ₂ H ₄ (+M)	5.600 × 10 ¹⁴	-0.414	66.0		[67]
		LOW F _c AR / 0.59 / N ₂ / 1 / O ₂ / 0.69 / NH ₃ / 4.87 /	1.600 × 10 ³⁴ 0.31	-5.490	1987.0	
R29	NH ₂ OH(+M) = NH ₂ + OH(+M)	1.400 × 10 ²⁰	-1.310	64080.0		[67]
		LOW F _c	5.400 × 10 ³⁷ 0.31	-5.960	66783.0	
R30	NH + OH = HNO + H	3.200 × 10 ¹⁴	-0.376	-46.0		[67]
R31	NH + OH = N + H ₂ O	1.600 × 10 ⁷	1.733	-576.0		[67]
R32	NH + H = N + H ₂	3.010 × 10 ¹³	0.000	0.0		[68]
R33	NH ₂ + NH = N ₂ H ₂ + H	1.500 × 10 ¹⁵	-0.150	0.0		[75]
R34	NH + NO = N ₂ O + H	2.700 × 10 ¹⁵	-0.780	20.0		[68]
R35	NH + NO = N ₂ + OH	6.800 × 10 ¹⁴	-0.780	20.0		[68]

(continued on next page)

Table 2 (continued)

ID	Reaction	A	β	E_{act}	Notes	Ref
R36	$N + OH = NO + H$	2.830×10^{13}	0.000	0.0		[68]
R37	$N + O_2 = NO + O$	9.027×10^9	1.000	6500.0		[68]
R38	$NO + N = N_2 + O$	9.400×10^{12}	0.140	0.0		[16]
R39	$H + O_2 (+M) = HO_2 (+M)$	4.650×10^{12}	0.440	0.0		[76]
R40	LOW	1.737×10^{19}	-1.230	0.0		
	F_c	0.67				
R40	$H_2 / 1.30 / CO / 1.90 / CO_2 / 3.80 / HE / 0.64 / H_2O / 10.00 / AR / 0.50 / CH_4 / 2.00 / C_2H_6 / 3.00 / H + O_2 = O + OH$	1.140×10^{14}	0.000	15286.0	$A \times 1.1$	[77]
R41	$H_2 + O = OH + H$	5.080×10^4	2.670	6292.0		[78]
R42	$H_2 + OH = H_2O + H$	4.380×10^{13}	0.000	6990.0		[79]
R43	$H + OH + M = H_2O + M$	3.500×10^{22}	-2.000	0.0		[80]
	$H_2 / 0.73 / H_2O / 3.65 / CH_4 / 2.00 / C_2H_6 / 3.00 / AR / 0.38 /$					

simulated as adiabatic batch reactors, with a time-dependent volume history, calculated through the assumption of isentropic compression from the pressure profiles experimentally obtained. The criterion for ignition delay time was coherent with the experimental one adopted in the reference works, i.e. the difference between the time at which the maximum pressure rise rate is recorded, and the time at the end of

compression. JSR simulations were performed by considering perfect mixing [82], isothermal conditions and a steady state. Finally, LFSs were calculated through the 1D, premixed laminar flame solver, using an adaptive grid, with a maximum allowed gradient and curvature coefficient between two adjacent points equal to 0.05 and 0.5, respectively. A continuation method was used to calculate LFS as a function of the

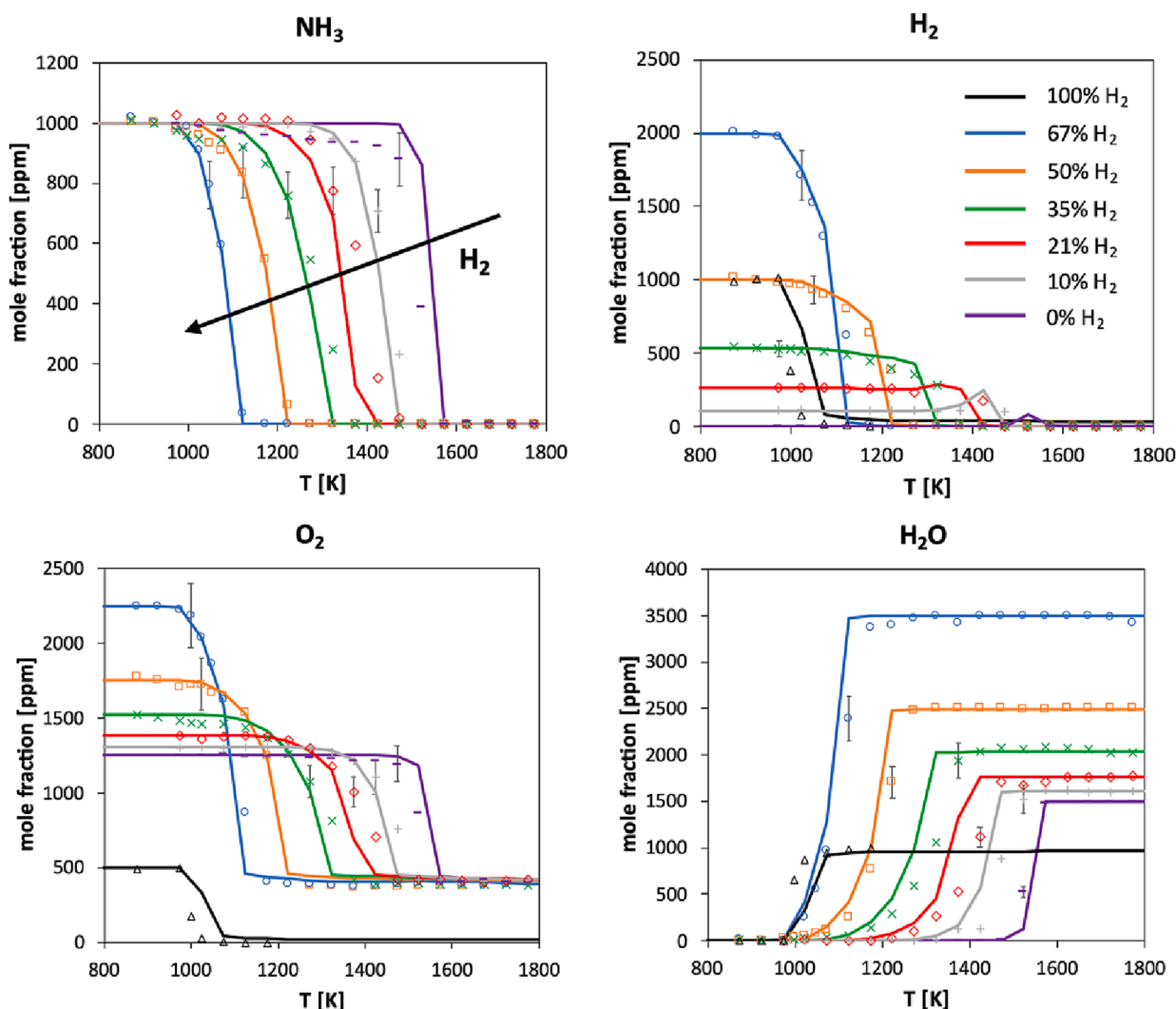


Fig. 1. Oxidation of NH_3/H_2 mixtures in a flow reactor (cfr. Table 1), at $\Phi_{NO} = 1$. Reactant consumption and H_2O formation. Experimental and modeling results.

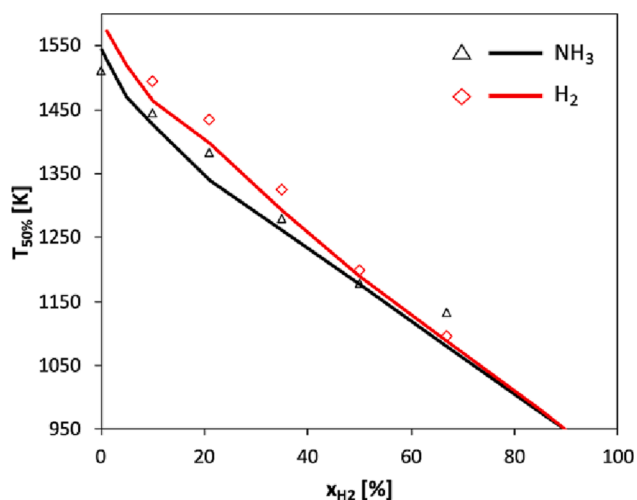


Fig. 2. Temperature at which 50% NH_3/H_2 conversion is reached, obtained via interpolation of experimental (symbols) and modeling (lines) results.

equivalence ratio. Radiation effects, which were recently shown to play a role in pure ammonia flames [83], were considered via an optically-thin model [84].

3. Results and discussion

In this section, the reactivity, the nitrogen fate and the mutual interaction between NH_3 and H_2 in the related blends is investigated in a wide range of operating conditions, in terms of temperature (T), pressure (P) and equivalence ratio (Φ). In particular, this study is focused on two major targets: i) the analysis of the low- and intermediate-temperature oxidation of NH_3/H_2 mixtures, and the kinetic pathways driving reactivity and nitrogen selectivity with a variable amount of hydrogen; ii) the kinetic analysis of non-linear effects on both reactivity and flame propagation, resulting from the progressive addition of hydrogen. Section 3.1 presents the experimental results obtained in the current experimental campaign, and the related kinetic analysis. Afterwards, Section 3.2 and 3.3 further deepen the low-temperature interaction between ammonia and hydrogen in mixtures with variable blends, by considering literature case studies, involving product quantification as measured in JSR and the ignition delay times as measured in RCMs, respectively. Finally, Section 3.4 completes the picture by shedding light on the chemical role of hydrogen in enhancing the laminar burning velocity of ammonia, through the kinetic analysis of freely

propagating flames recently studied experimentally.

3.1. Intermediate-temperature: oxidation in a flow reactor

Fig. 1 shows the effect of the progressive addition of hydrogen on the reactivity of ammonia and the formation of water. As expected, increasing amounts of hydrogen shift the reactivity towards lower temperatures, while the profiles are qualitatively similar and the consumption rate of NH_3 as a function of the temperature is comparable in all the cases.

Concerning H_2 , as soon as its amounts are low, it starts being consumed at higher temperatures, later than ammonia. Such a difference becomes negligible for $x_{\text{H}_2} \geq 50\%$. This trend is mostly related to the fact that H_2 is also an intermediate product in the oxidation path of NH_3 [20], which explains the peak in its mole fraction that can be observed for pure NH_3 and to a larger extent for $x_{\text{H}_2} = 10\%$. Fig. 2 summarizes this behavior by showing the temperatures, at which the two fuels reach a 50% conversion ($T_{50\%}$). For a more complete overview of this trend, NH_3/H_2 mixtures were simulated also outside of the experimental range ($0.01 \leq x_{\text{H}_2} \leq 0.85$). The rate of reduction in $T_{50\%}$ with x_{H_2} is maximum with pure NH_3 , then converging to a linear trend for $x_{\text{H}_2} \geq 10\%$, with the two fuels reaching a common $T_{50\%}$ for high H_2 amounts.

For all of the considered datasets, the kinetic model is able to reasonably predict the experimental trends, in terms of both species profiles and $T_{50\%}$. Regarding species profiles, it is worth noticing the prediction of a peak in the H_2 mole fraction for $x_{\text{H}_2} \leq 21\%$, before its consumption, thus pointing out a chemical interaction between both fuels. In order to understand this, Fig. 3a shows the evolution of the predicted H_2 mole fraction over the reactor length, for $x_{\text{H}_2} = 10\%$ and $T = 1423$ K. As shown in the rate of production analysis (ROPA) reported in Fig. 3b, as soon as the H atom is formed at the reactivity onset, H_2 is first formed from the H-abstractions by the H atom itself on the nitrogenated species, thus it starts accumulating. Afterwards, when a sufficient pool of O and OH radicals is available, it starts reacting through the usual branching path. Therefore, the overlapping of hydrogen formation as an intermediate before its reaction slows down its consumption rate when in mixtures. This also explains the delayed $T_{50\%}$ for H_2 (Fig. 2), if compared to NH_3 .

Fig. 4 provides a general picture of the chemical interaction between the two fuels: here, the sensitivity analysis to NH_3 mass fraction, performed in comparable conditions (1% ammonia conversion), highlights that ammonia consumption is mostly controlled by H-abstractions from the fuel. In the absence of hydrogen, reactivity is triggered by the H-abstraction by O_2 (R5), acting as an initiator of the whole process

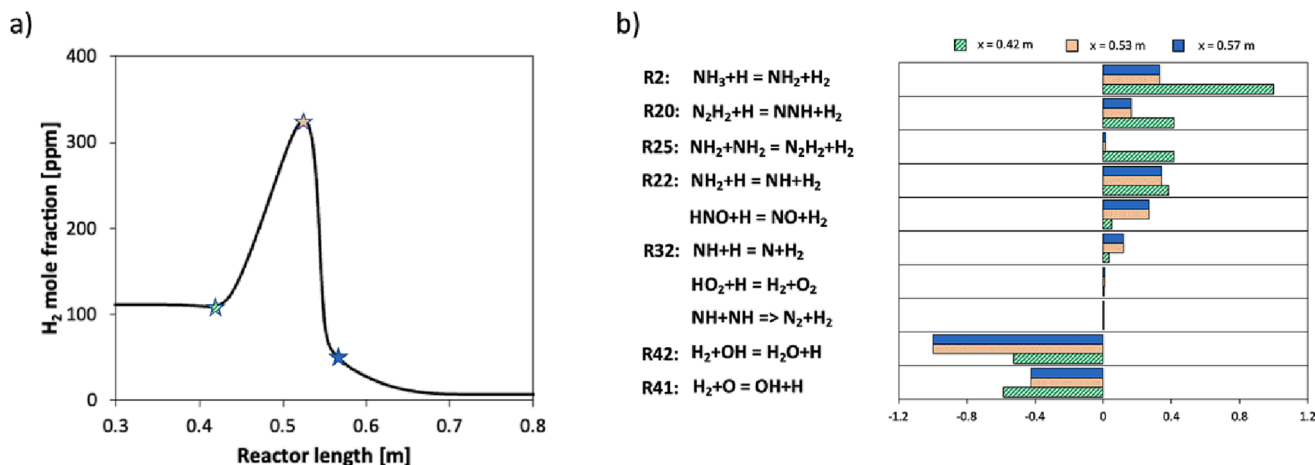


Fig. 3. A) predicted hydrogen mole fraction through the reactor length. b) rate of production analysis for H_2 in three characteristic points indicated by the stars. $T = 1473$ K. $x_{\text{H}_2} = 10\%$.

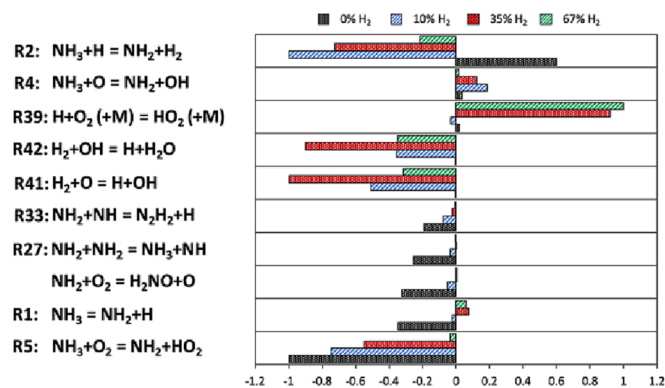


Fig. 4. Sensitivity analysis to NH₃ mass fraction for the different mixtures, normalized with respect to the maximum value (at 1% ammonia conversion). The reaction R40 is omitted.

(together with the fuel thermal decomposition R1, playing a minor role though, because of the relatively low temperatures). With the same composition, the H-abstraction by the H radical (R2) plays an inhibiting effect, since it subtracts H atoms from the radical pool, providing NH₂, less reactive. Interestingly, when hydrogen is added (especially in small amounts), R2 enhances ammonia conversion instead. Such an inversion can be attributed to the fact that the availability of H atoms is no longer

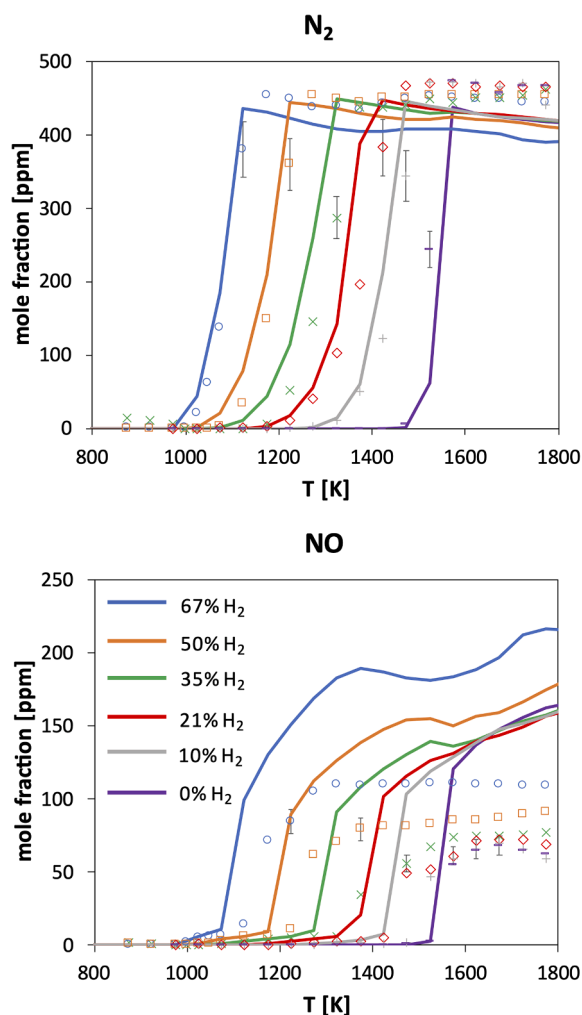


Fig. 5. Oxidation of NH₃/H₂ mixtures in a flow reactor (cfr. Table 1), at $\Phi_{NO} = 1$. NO and N₂ formation. Experimental and modeling results.

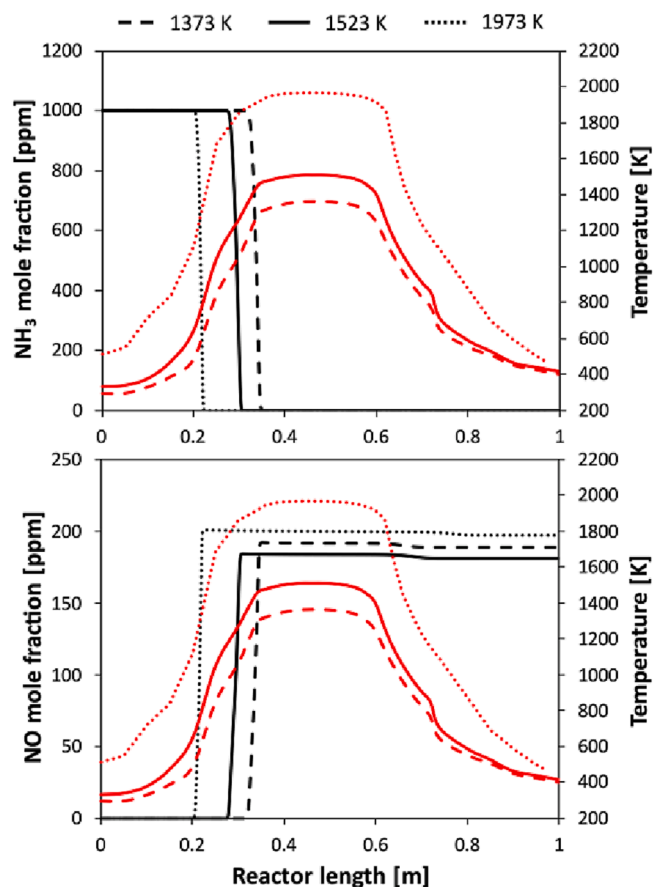


Fig. 6. Predicted NH₃ consumption and NO formation (black lines), and measured temperature profiles (red lines), throughout the reactor length for three nominal temperatures. ($x_{H_2} = 0.67$, $\Phi_{NO} = 1$). (For interpretation of the references to colour in this figure legend, the reader is referred to the web version of this article.)

limited by such a reaction, since they are rather provided by the direct oxidation of H₂. In this way, the addition of H₂, even in small amounts, acts as a flywheel for ammonia oxidation: as shown in Fig. 2, with small amounts of hydrogen (up to 10%), the effect on the anticipation of reactivity is stronger, then becoming approximately linear for $x_{H_2} > 10\%$. The remaining H-abstractions (R3 to R6) slow down the reactivity onset, too, when hydrogen is added, while being not particularly relevant with pure ammonia. The same occurs for the third-body reaction R39, acting as a termination, in competition with the branching reaction R40, not shown in Fig. 4 for the sake of readability, as it always exhibits the maximum (negative) sensitivity coefficient.

In parallel to the reactant consumption and water formation, Fig. 5 shows the nitrogen fate in terms of N₂ and NO mole fractions. Regardless of the initial fuel mixture, most nitrogen is converted into N₂. The experimental data show that, after the complete conversion of ammonia is reached, the amounts of N₂ and NO are fairly stable with the increasing temperature, and the variation of the respective mole fractions are much lower than the experimental uncertainty. In terms of nitrogen conversion and NO yield (referred to nitrogen), evaluated as:

$$\eta_{NO} = \frac{X_{NO}}{X_{NH_3} + 2 \cdot X_{N_2} + X_{NO}} \quad (3)$$

the 6 experimental datasets suggest that the addition of hydrogen to the fuel mixture increases the NO yield from ~5% to ~10% in a monotonic way.

From a modeling standpoint, results are still reasonable with regard to N₂ mole fraction, and within the 10% uncertainty. Concerning NO

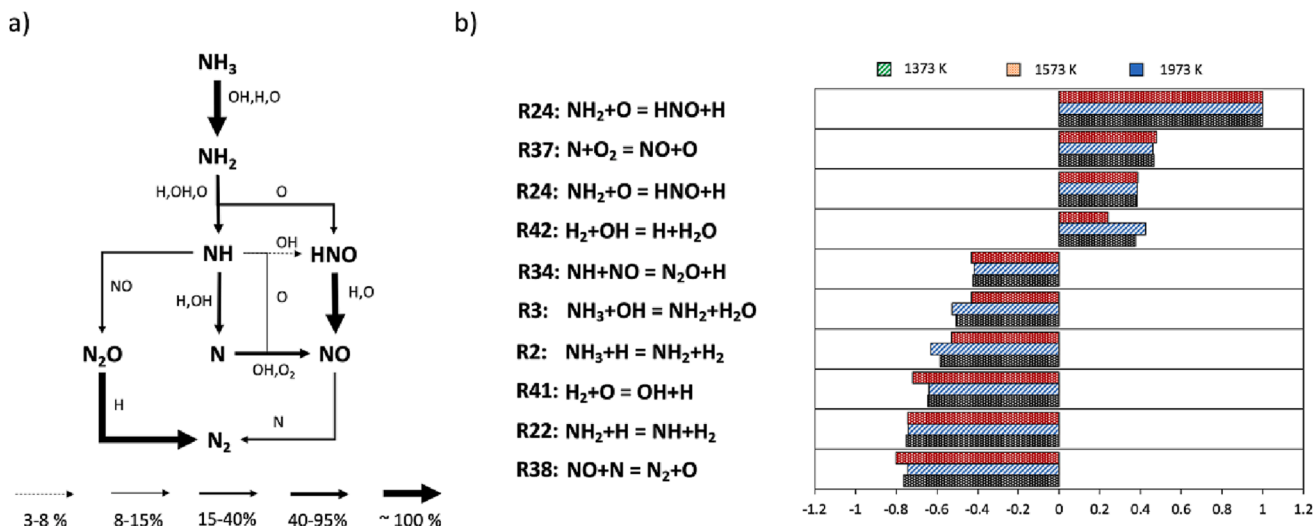


Fig. 7. a) reaction flux analysis for nitrogen containing species in fr at $t = 1573$ K. b) Sensitivity analysis to NO mass fraction, normalized with respect to the local maximum reaction rate (reaction R40 was omitted). Both diagrams were evaluated at 99% max NO mole fraction ($x_{\text{H}_2} = 0.67$, $\Phi_{\text{NO}} = 1$).

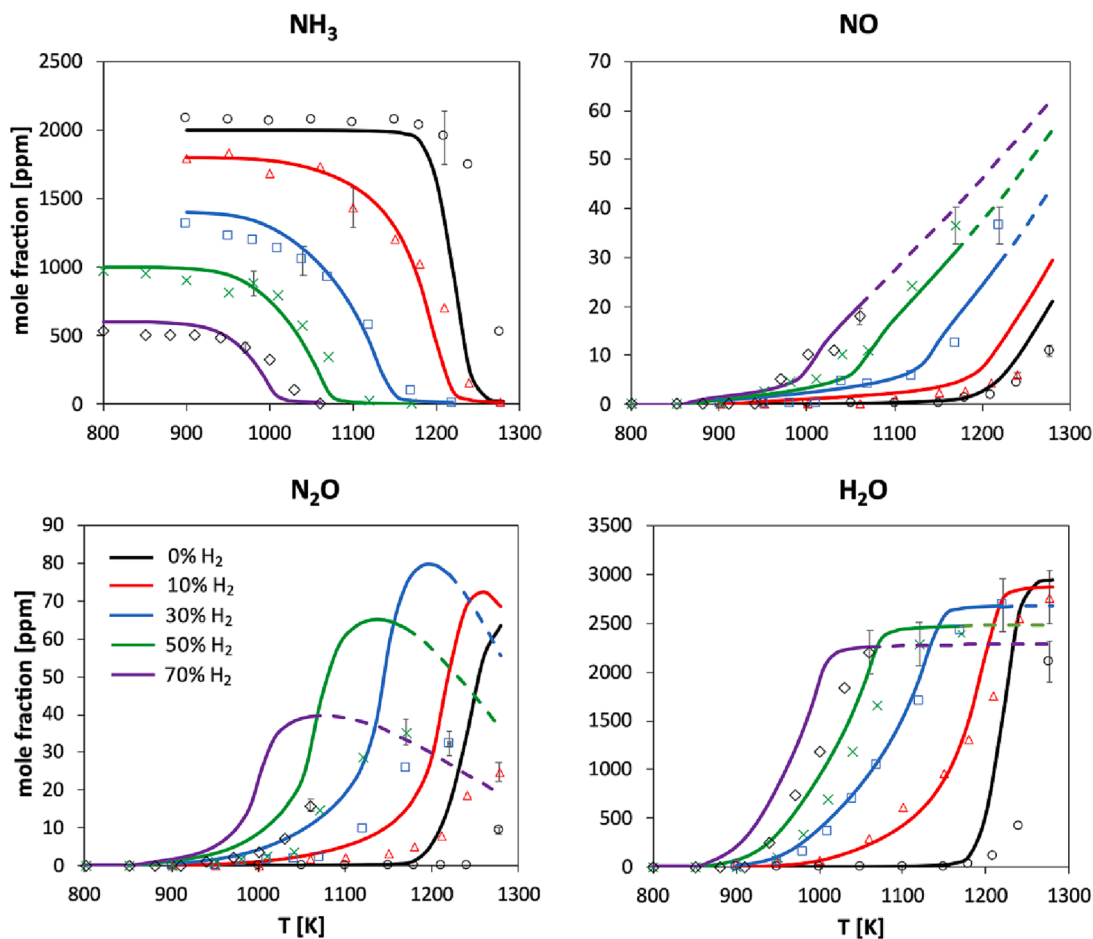


Fig. 8. Mole fraction profiles in the oxidation of $\text{NH}_3/\text{H}_2/\text{O}_2/\text{N}_2$ mixtures in a JSR. $P = 1$ atm. $\Phi_{\text{NO}} = 0.25$. $\tau = 1$ s. Experimental [49] vs modeling results (dashed lines are predictions outside the experimental range).

formation, three major points must be emphasized: i) especially for the lowest amounts of hydrogen, an overprediction up to a factor 2 is present at the highest temperatures, which is reduced to a factor ~ 1.5 by increasing the hydrogen amount. Qualitatively, this is in line with the performance of the same model in a previous study performed in a FR

with pure NH_3 [20]. ii) The non-monotonic trend is no longer retained with increasing the H_2 amount in the fuel mixture, as at the highest temperatures an inversion is observed for the mixtures with lower amounts of hydrogen. iii) Considering the fuel mixtures richest in hydrogen ($x_{\text{H}_2} \geq 35\%$), the predicted NO mole fraction is non-

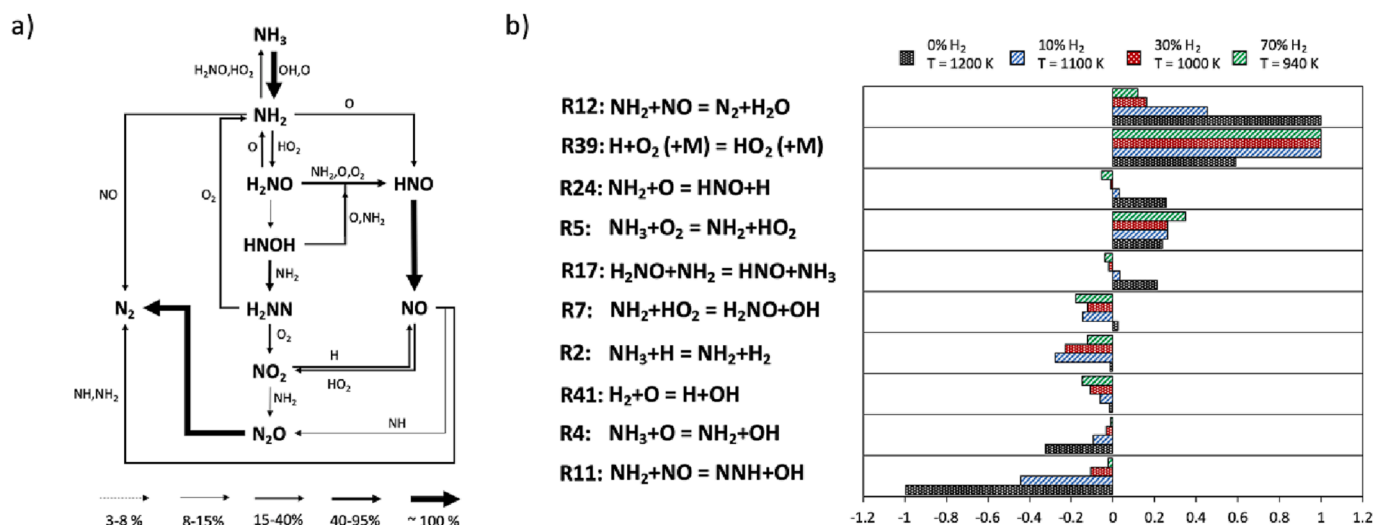


Fig. 9. a) reaction flux analysis for nitrogen-containing species (30% h_2 - $T = 1050$ K - $\Phi_{\text{NO}} = 0.25$). b) Sensitivity analysis to NH_3 mass fraction in the oxidation of $\text{NH}_3/\text{H}_2/\text{O}_2/\text{N}_2$ mixtures in a JSR (Fig. 8), normalized with respect to the local maximum value in correspondence of $\sim 10\%$ conversion. The reaction R40 is omitted.

monotonic with the temperature, exhibiting a minimum between 1400 K and 1600 K, which is not observed experimentally. Comparable trends can be obtained by using independent literature mechanisms available in literature [15,49,61,85], as shown in Figs. S2–S5 in the SM. This is the most critical aspect of the numerical predictions, certainly counterintuitive since NO formation is kinetically favored with the temperature due to the thermal NO_x mechanism [86]. To shed light on this behavior, the predicted consumption of NH_3 and formation of NO throughout the reactor length was investigated in the most critical subset, i.e. with 67% H_2 as fuel. Fig. 6 illustrates the results, where the measured temperature profiles are also shown for completeness. The three profiles highlight that the presence of H_2 within the fuel shortens the ignition time of the fuel mixture, to the extent that, starting from 1373 K, this occurs in the pre-heating region. Above all, Fig. 6 shows that NO is formed during ignition (i.e. when N_xH_y radicals are available for the fuel- NO_x mechanism), finally reaching a plateau. As a result, the amount of produced NO depends on the ignition temperature: on turn, this is the result of the heating history, not strictly correlated to the nominal temperature. The $T_{50\%}$ of NH_3 are indeed equal to 1269 K, 1244 K and 1289 K for the three temperatures, respectively: such an order is coherent with the amount of produced NO.

The flux analysis of nitrogen-containing species at 1573 K (Fig. 7a) shows that NO formation occurs via two parallel pathways, i.e. via the

H-abstractions on the HNO intermediate and the oxidation of the N radical (thermal- NO_x). Only at a second stage, NO is reduced to N_2 , after further reacting with either NH (R35) or N (R38) radicals. Sensitivity analysis to NO mass fraction (Fig. 7b) corroborates the role of such paths in driving NO formation, and highlights that, on a relative scale, they are comparable at the different temperatures, both qualitatively and quantitatively. In particular, the prior conversion of NH_2 to HNO (R24) is the major enhancer of its formation, in accordance to what already observed in a recent work [20] for the oxidation of pure ammonia. With regard to R24, it is also important to highlight that significant uncertainty persists on its available theoretical [73,87] and experimental [88,89] estimations. On the other hand, it is interesting to notice that the thermal- NO_x reactions are in competition between each other, since the oxidation of the N radical via either OH (R36) or O_2 (R37) promotes NO formation, while the third one (R38) contrasts this process by acting in the direction of NO reduction. The underlying reason of such a behavior must be sought in the origin of N radicals, ultimately bringing to NO: while with conventional hydrocarbons, they are provided by breaking the atmospheric nitrogen, in this case they rather come from the fuel itself, thus their availability does not require such high temperatures as in the usual formation via the thermal pathway. Also, once NO is available, diatomic nitrogen can be formed through its reduction. The absence of nitrogen in the reacting mixture (experiments were performed in a helium

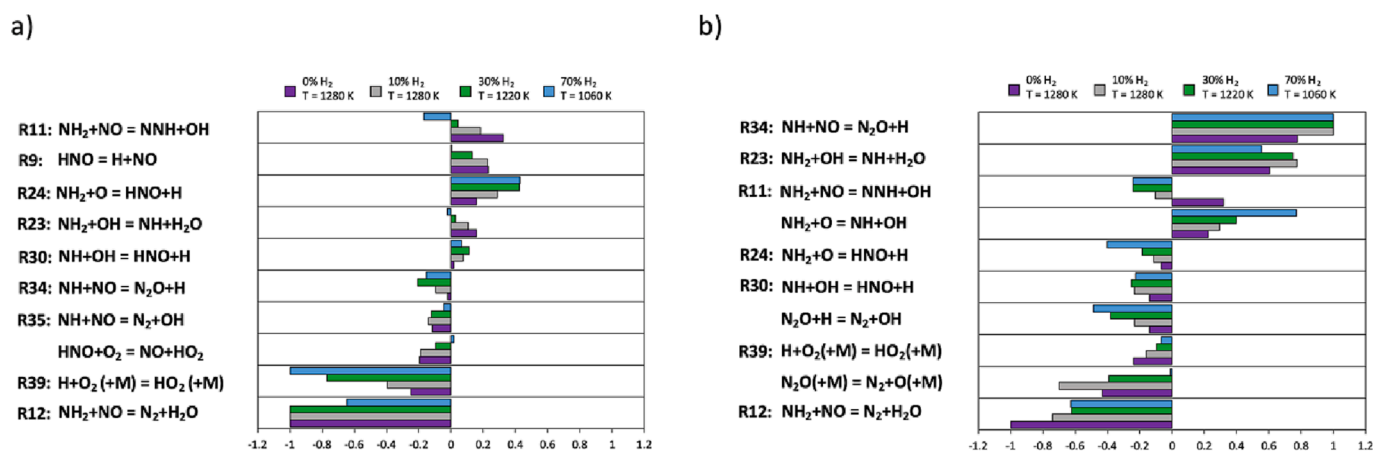


Fig. 10. Sensitivity analysis to a) NO and b) N_2O mass fractions in the oxidation of $\text{NH}_3/\text{H}_2/\text{O}_2/\text{N}_2$ mixtures in a JSR (Fig. 8), normalized with respect to the local maximum values, at the highest temperature of each experimental data series.

environment) enhances this process from a thermodynamic standpoint.

3.2. Lower-temperature: oxidation in a jet-stirred reactor

In order to highlight the features of the intermediate-temperature regime analyzed in Section 3.1, the lower-temperature experiments of ammonia-hydrogen mixtures recently performed in a JSR by Zhang et al. [49] were considered. Lean and stoichiometric conditions, at atmospheric pressure, were explored ($\Phi_{\text{NO}} = 0.25$ and $\Phi_{\text{NO}} = 1$), using nitrogen as balance gas. Fourier-transform infrared (FTIR) spectroscopy was used for the identification and the quantification of species (NH_3 , H_2O , NO and N_2O). This technique does not allow to detect homonuclear diatomic species like N_2 and H_2 . Fig. 8 shows the results for the leaner compositions (the remaining datasets are presented in SM), in terms of NH_3 consumption and water formation, as well as nitrogen fate (NO , N_2O). In this case, too, the kinetic model well predicts the reactivity trends as a function of the blending ratio, except for an earlier onset with pure ammonia. An approximately linear decrease in the $T_{50\%}$ can be observed for all the blending ratios. Moreover, the NH_3 consumption rate with the temperature is less steep with higher H_2 fractions, whilst being more abrupt in the pure case. Indeed, a gradual shift from ammonia to hydrogen chemistry can be observed in the nitrogen flux analysis and sensitivity analysis to NH_3 mass fraction (Fig. 9). Pure ammonia consumption is regulated by the competition between the “thermal-De NO_x ” reactions (R11 and R12). Coherently with the past work [20], and in contrast with the flow reactor (Section 3.1) where it initiates the fuel conversion, the H-abstraction from NH_3 by O_2 (R5) slows down the oxidation process with all the blending ratios, by acting in the reverse direction due to the relative abundance of HO_2 at lower temperatures. The key role of the H_2NO intermediate in NH_3 oxidation is also confirmed in both flux and sensitivity analysis: it is generated via the $\text{NH}_2 + \text{HO}_2$ propagation path (R7), then it is converted to HNO via the related H-abstractions (R17 and R18). In particular, R17 slows down reactivity, to a significant extent, with pure ammonia, whilst becoming negligible with the addition of hydrogen.

On the other hand, Fig. 8 also shows that NO formation is well predicted by the kinetic model at the different temperatures, while N_2O is overpredicted at all blending ratios, up to a factor ~ 2 . The fate of nitrogen was further investigated via sensitivity analysis, in order to understand the kinetic competitions in NO and N_2O formation. Fig. 10 shows the controlling reactions for NO and N_2O , respectively. Regarding NO , its formation is mostly driven by the oxidation of NH_x radicals to HNO , on turn providing NO as already shown in Fig. 7a. The competition between R39 and R40 regulates the radical pool amount ($\text{H}/\text{O}/\text{OH}$), such that, as expected, NO increases with temperature. On the other hand, NO formation is inhibited by the reduction of NO itself with NH_x radicals, occurring via R34 and R12, providing N_2 and N_2O , respectively. In particular, R34 results in a competition between NO and N_2O ,

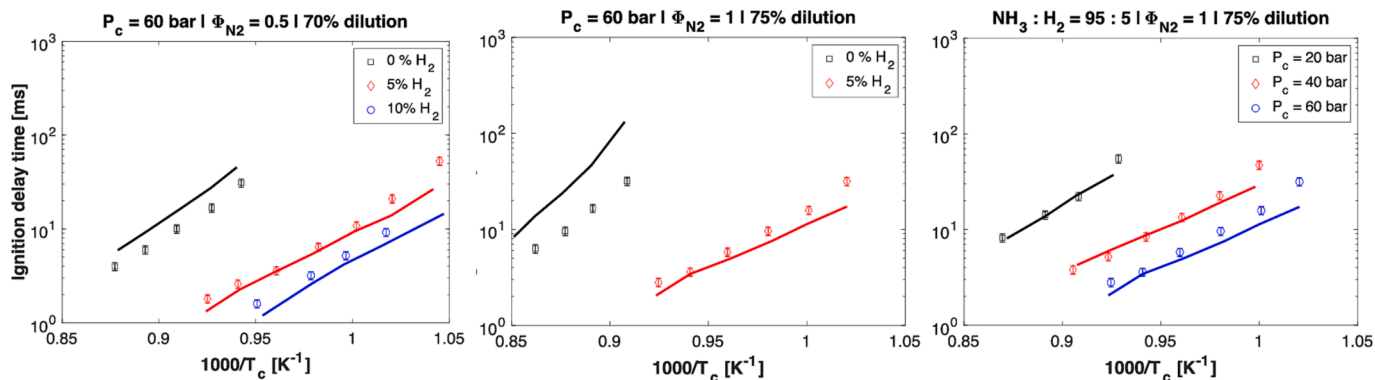


Fig. 11. Ignition delay times of NH_3/H_2 mixtures in a rapid compression machine. Experimental data (cfr. Table 1 of [46]) vs modeling results. Volume histories were obtained through private communication from the authors of [46].

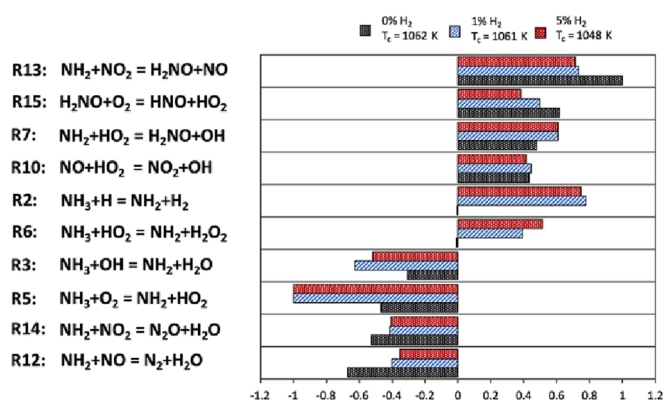


Fig. 12. Sensitivity analysis to OH mass fraction in the oxidation of $\text{NH}_3/\text{H}_2/\text{O}_2/\text{Ar}/\text{N}_2$ mixtures in a Rapid Compression Machine (Fig. 11– $\Phi = 0.5$), normalized with respect to the local maximum values, in correspondence of 1% NH_3 conversion.

and indeed it is one of the most important reactions bringing to the formation of N_2O , as shown in Fig. 10b. R34 is one of the two channels resulting from the reaction of NH with NO , the second being R35. Their branching ratio (80% towards R34) was recommended by Baulch et al. [68], and adopted also in [15,49]. Therefore, considering R34 and R35, the predictive features with respect to the two datasets are antagonistic to each other.

The second key reaction driving N_2O formation is the conversion of NH_2 to NH via R23. Since such a path brings to the formation of NH and subsequent conversion to N_2O via R34, Fig. 10b shows that R23 has an importance comparable to the former, while being not particularly relevant in the formation of NO . The kinetic model adopts the rate proposed by Li et al. [66], which is 20% lower than the value proposed by Klippenstein et al. [67], and a factor 3 lower than the evaluation by Mousavipour et al. [90] at 1000 K, thus providing the closest predictions to the experimental data.

3.3. Lower-temperature: ignition in a rapid compression machine

The importance of low- and intermediate-temperature chemistry of ammonia, and related interaction with hydrogen becomes even more emphasized at high-pressure conditions, typical of internal combustion engines and gas turbines. Several studies were recently performed in different RCMs [45–47] in lean-to-rich conditions, using nitrogen and/or argon as balance gases. Although such devices involve non-ideal features related to gas motions and heat losses, most often requiring the simulation via Computational Fluid Dynamic (CFD) models and detailed kinetics [91], the adoption of the adiabatic-volume assumption allows for a significant model simplification, thus reducing the problem

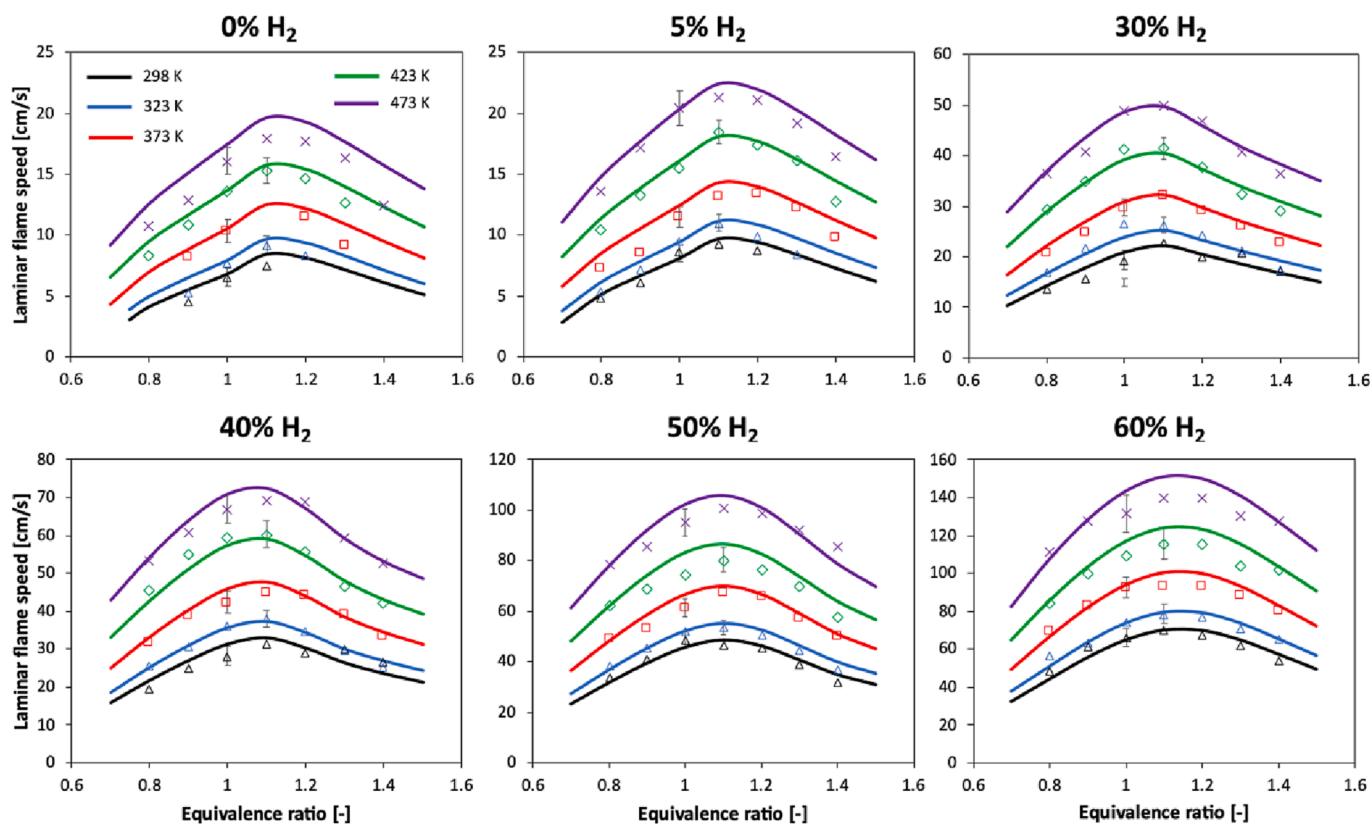


Fig. 13. Laminar flame speeds of $\text{NH}_3/\text{H}_2/\text{air}$ mixtures at atmospheric pressure, and variable unburned gas temperature T_u and Φ_{N_2} . Experimental data (symbols) [57] vs modeling results (lines).

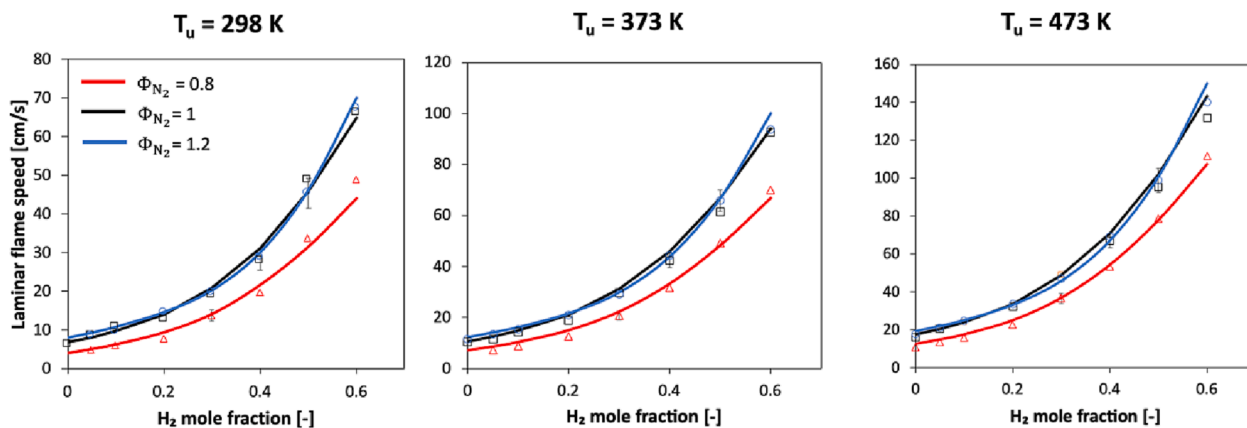


Fig. 14. Laminar flame speeds of $\text{NH}_3/\text{H}_2/\text{air}$ mixtures at atmospheric pressure and variable T_u , as a function of the hydrogen mole fraction. Experimental data (symbols) [57] vs modeling results (lines).

to a 0-dimensional one. Therefore, even if using RCM data for kinetics development would not be fully appropriate, since chemistry is coupled to boundary-layer effects, using a 0D reactor with an assigned volume profile provides a first benchmark of the mechanism performance.

Fig. 11 provides a parametric comparison of modeling predictions in lean conditions at different compression pressures and variable x_{H_2} , with variable hydrogen amounts (datasets by Pochet et al. [45] and He et al. [47] are shown in the SM). Mixed results can be observed, even in comparable conditions: considering the data by Dai et al. [46], a very reasonable agreement with the experimental IDTs can be observed for all the NH_3/H_2 mixtures, while the IDT of pure ammonia is underestimated. Yet, as can be seen by reproducing the datasets of Pochet et al. [45] and He et al. [47] (shown in the SM), retaining the generality

feature in the whole parametric space and considering different experimental RCMs is a challenging task. In the case of Pochet et al. [45], in lean conditions the reactivity of NH_3/H_2 mixtures is overestimated, while in the case of He et al. [47], previous works [45,47,49] pointed out that no kinetic mechanism is able to keep the generality feature with varying equivalence ratio and blending ratio: the considered mechanisms mostly differ by their relative reactivity, according to their core NH_3 chemistry.

In this case, too, sensitivity analysis was leveraged to understand the changes in the paths controlling IDTs with the hydrogen amount. Fig. 12 shows the relevant paths in determining OH mass fraction, considered as a marker of IDT. The main deduction that can be drawn is that ammonia sub-chemistry is the sole controlling one, and specifically i) H-

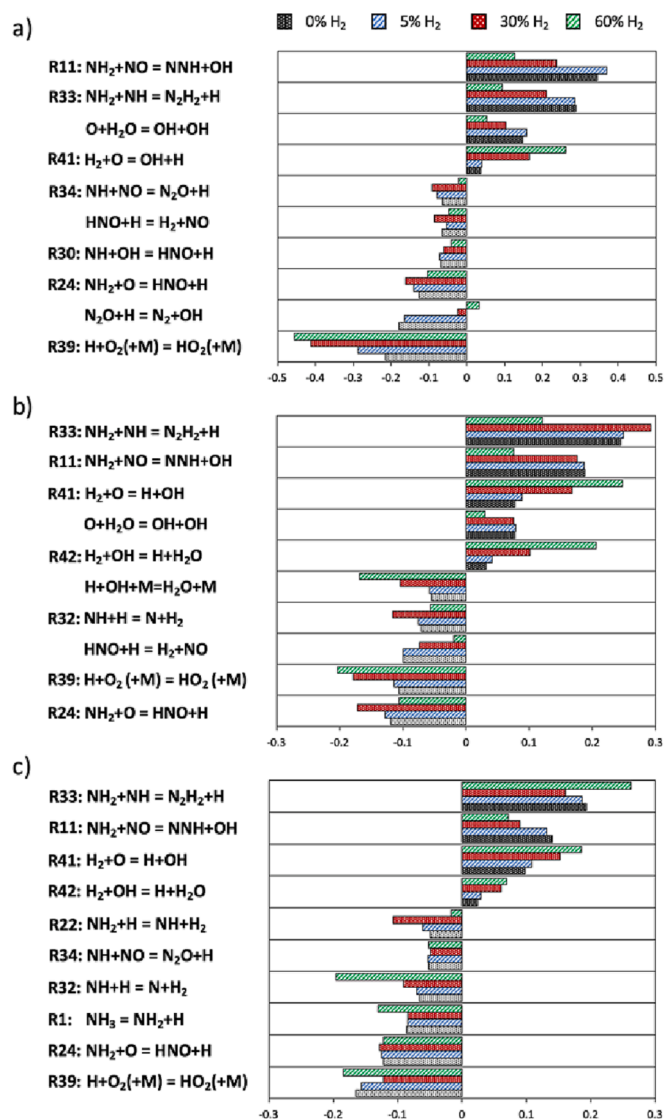


Fig. 15. Sensitivity analysis to the laminar flame speed at $T_u = 298$ K and variable hydrogen fractions, normalized with respect to the sensitivity coefficient of R40 (not shown). a) $\Phi = 0.7$, b) $\Phi = 1$, c) $\Phi = 1.5$.

abstractions from NH_3 , ii) $\text{NH}_2 + \text{NO}_x$ channels and iii) H_2NO chemistry.

With regard to H-abstractions, R2 has a comparable role to what already found in the flow-reactor experiments performed for this work (Fig. 4): supposedly for the same reason as in the FR case (higher availability of H radicals provided by H_2) for increasing oxygen amounts, R2 is a reactivity enhancer, while being not significant in the absence of H_2 . The remaining H-abstractions, by OH (R3) and O_2 (R5), are reaction inhibitors, but for different reasons: on the one hand, the abstraction by OH subtracts active radicals from the radical pool, and slows down the branching process. On the other hand, R5 act as termination reactions due to the abundance of HO_2 radicals, as already observed at lower temperatures in JSR experiments (Section 3.2), and unlike intermediate-temperature FR datasets (Section 3.1). Concerning $\text{NH}_2 + \text{NO}_x$ reactions, the temperature range is favorable for the competition between R11 and R12 (thermal DeNO_x [15,20,92]), while the high pressures at stake favor the presence of NO_2 , thus determining the parallel competition between R13 and R14. In particular, the propagation channel R13 leads to the H_2NO intermediate (along with R7), whose major role at low temperatures has been already pointed out in Section 3.2, and in previous works [20,59]. Especially with low or no hydrogen, its oxidation to HNO is indeed one of the major reactivity

enhancers.

Interestingly, the rate of almost all the controlling reactions identified in Fig. 12 is either the result of high-level theoretical calculations (R2, R3, R5, R6, R12, R13, R14, R15), or is well consolidated in literature, as is the case of R10.

3.4. Role of hydrogen addition on laminar burning velocity

Accurately representing the interaction between ammonia and hydrogen in the related blends becomes critical when flame propagation features are investigated. In the latest years, plenty of data have been collected with regard to the laminar flame speed of ammonia blends with hydrogen and/or other hydrocarbons, for which the kinetic mechanisms are well established. As shown by Han et al. [56,93], the behavior with the amount of added species depends on the species itself: regarding hydrogen, a more-than-linear increase with the hydrogen mole fraction has been identified.

In order to get an insight on the chemical couplings behind such a behavior, hereafter a modeling investigation of the experimental data recently obtained by Lhuillier et al. [57] is presented. Such a study includes a parametric investigation of the laminar flame speed of NH_3/H_2 mixtures at atmospheric pressure, with variable i) unburned temperature T_u , ii) hydrogen amount x_{H_2} and iii) equivalence ratio Φ (evaluated according to (2)). Fig. 13 shows that a very good agreement is reached in the whole ($T_u, x_{\text{H}_2}, \Phi$) space. No systematic under- or overestimations can be identified, and as shown in Fig. 14, the non-linear increase in the flame speed with the oxygen amount is predicted very well, at the different Φ and T_u , where the deviations are well within the experimental uncertainty.

To shed light on the chemistry driving the more-than-linear increase in the laminar flame speed with the hydrogen mole fraction, sensitivity analysis was performed at a sample T_u and three representative Φ , and the behavior of sensitivity coefficients with the mixture composition was investigated. Fig. 15 shows the results, where sensitivity coefficients were normalized with respect to those of the branching reaction R40 used as reference. Regardless of the equivalence ratios, two trends can be clearly identified. First of all, the importance of $\text{NH}_2 + \text{NO}$ propagation channel (R11), providing OH radicals, quickly decreases with increasing x_{H_2} , as it is no longer the major source of the radical pool. The same occurs for the $\text{NH}_2 + \text{NH}$ propagation path via R33 at lean conditions, while at stoichiometric and rich conditions it keeps playing a major role, due to the higher availability of NH_x radicals. On the other hand, the importance of H_2/O_2 chemistry becomes predominant in controlling the flame speed, in particular the H-abstractions R41 and R42 generating H radicals, on turn branching via R40, and R39 stopping reactivity as it subtracts H atoms from the pool, terminating into a much less reactive HO_2 . The same holds for the third-body termination R43. Combining R41 and R42 with R40 results in a radical branching process boosting the laminar flame speed because of the more-than-linear increase of radicals caused by R40, and the higher availability of H_2 further speeds up R41 and R42.

Finally, within the NH_3 submechanism, it is worth noticing that the inhibiting effect of R24 persists at all the considered compositions. This had been already observed for pure ammonia mixtures [20], but it is interesting to notice that the behavior of R24 differs from, e.g., R11 in the NH_3 subset. Indeed, when hydrogen is present, R24 subtracts O radicals from the hydrogen oxidation path, thus competing with R41 which acts instead as a reactivity enhancer. It is worth highlighting that R24 was also found to be critical for NO predictions (Section 3.1), and considering the uncertainty around it, further studies on it would be beneficial to reconcile both NO speciation and laminar flame speed. On the other hand, R1 acts in the reverse direction as a termination, thus scavenging H radicals even when hydrogen predominates.

4. Conclusions

Unraveling the chemical interactions between ammonia and hydrogen is an essential requirement for mapping the behavior of the binary blends in the whole operating space, and allowing a flexible use for a variety of applications. In this work, light was shed on the low- and intermediate-temperature oxidation of NH_3/H_2 mixtures with a variable blending ratio. To this purpose, an experimental and modeling study was performed, by combining new data, collected in a flow reactor at intermediate temperatures, with the most recent literature datasets. These were obtained in different devices (jet-stirred reactor, rapid compression machines, laminar flames), thus covering all the conditions of interest, as well as the major combustion features (ignition, flame propagation). At the same time, an established kinetic mechanism, previously developed for ammonia oxidation, was revised according to the recent theoretical findings, and leveraged to interpret the obtained results: rate of production, flux and sensitivity analysis were the kinetic tools to identify the binary interactions, and the role of the most critical reaction steps, deserving a deeper theoretical attention in future studies.

The newly-collected datasets, covering the whole transition from pure NH_3 to pure H_2 , were coherently reproduced by the kinetic model for what concerns the reactivity onset and water formation. When adding hydrogen, the half-conversion temperature was shown to be anticipated in a linear way with the hydrogen mole fraction, except for the smallest amounts, where the anticipation rate was faster. The kinetic analysis allowed to gain an insight in the changes occurring from pure NH_3 to binary mixtures: the opposite role played by H-abstraction by the H radical from NH_3 could be highlighted, first inhibiting then enhancing reactivity, due to the availability of H atoms from the direct oxidation of H_2 . Concerning the nitrogen fate, most of it was converted to N_2 (>90%), while the rest was NO, which was found to increase monotonically with the hydrogen fraction. On the other hand, the amounts predicted by the mechanism were i) up to a factor 2 larger than what measured (as already found in previous works with pure ammonia [20]), ii) converging to comparable values at high temperature for all the compositions (except for the mixture richest in H_2), and iii) non-monotonic with the temperature for the largest hydrogen amounts. Although the third outcome might seem counterintuitive, a deeper analysis in the conversion history within the reactor could attribute NO oscillations at high temperatures to an early mixture ignition in the pre-heating region due to the increased reactivity when hydrogen was added, such that the final results became strictly dependent on the heating history (i.e. temperature profile).

The analysis was then extended to lower temperatures, considering the datasets recently collected in a Jet-Stirred Reactor at atmospheric pressure. The key role of HO_2 was confirmed for the binary mixtures, too, due to the $\text{NH}_2 + \text{HO}_2$ reaction and its propagation and termination channels, whose relative ratio was found to control the fuel conversion rate. In this case, nitrogen selectivity was critical, though, and N_2O production was overestimated. Sensitivity analysis showed a major role for the $\text{NH} + \text{NO}$ reaction in these conditions, as its propagation channel results in the conversion of NO to N_2O . Further kinetic-modelling work might improve such predictions, although it should be considered that improvements in this regard are antagonistic with NO predictions in the already mentioned flow reactor conditions, thus causing a further overestimation. The low-temperature overview was then completed by the ignition delay time prediction in rapid compression machine. In addition to HO_2 as key radical, due to the high pressures, it was found that, even with small additions of hydrogen, the formation of NO_2 became relevant, paving the way to H_2NO through the $\text{NH}_2 + \text{NO}_2$ propagation channel, thus enhancing reactivity. Nevertheless, it was confirmed that being predictive on this kind of data remains a challenging task. In the future, the use of more complex RCM models, accounting for the thermal non-idealities, might shed further light in this direction.

Finally, the wide-range analysis of NH_3/H_2 interaction was

concluded by untangling the flame propagation behavior, and the superlinear increase in the laminar flame speed with the hydrogen mole fraction. It was shown that, as the main source of H radicals shifts from ammonia to hydrogen chemistry, the importance of H-abstractions from H_2 itself becomes predominant in releasing H atoms, thus driving the flame propagation. The combination of such effect to the branching reaction $\text{H} + \text{O}_2 = \text{O} + \text{OH}$ returns results in an explosive effect on the radical pool.

Declaration of Competing Interest

The authors declare that they have no known competing financial interests or personal relationships that could have appeared to influence the work reported in this paper.

Data availability

Experimental data and kinetic mechanism in CHEMKIN format are available as Supplementary Material of this work

Acknowledgements

This work has been carried out under the financial support of the IMPROOF project (H2020-IND-CE-2016-17/H2020-SPIRE-S016) within the European Union Horizon 2020 research and innovation program (grant agreement no. 723706), and of the COST Action CM1404 "Chemistry of smart energy carriers and technologies".

Appendix A. Supplementary data

Supplementary data to this article can be found online at <https://doi.org/10.1016/j.cej.2023.144577>.

References

- [1] K. Mazloomi, C. Gomes, Hydrogen as an energy carrier: prospects and challenges, *Renew. Sustain. Energy Rev.* 16 (2012) 3024–3033, <https://doi.org/10.1016/j.rser.2012.02.028>.
- [2] J. Eppinger, K.-W. Huang, Formic acid as a hydrogen energy carrier, *ACS Energy Lett.* 2 (2017) 188–195, <https://doi.org/10.1021/acseenergylett.6b00574>.
- [3] D. Miura, T. Tezuka, A comparative study of ammonia energy systems as a future energy carrier, with particular reference to vehicle use in Japan, *Energy*. 68 (2014) 428–436, <https://doi.org/10.1016/j.energy.2014.02.108>.
- [4] M. Meinshausen, N. Meinshausen, W. Hare, S.C.B. Raper, K. Frieler, R. Knutti, D. J. Frame, M.R. Allen, Greenhouse-gas emission targets for limiting global warming to 2 °C, *Nature*. 458 (2009) 1158–1162, <https://doi.org/10.1038/nature08017>.
- [5] Y. Kojima, Hydrogen storage materials for hydrogen and energy carriers, *Int. J. Hydrogen Energy*. 44 (2019) 18179–18192, <https://doi.org/10.1016/j.ijhydene.2019.05.119>.
- [6] G. Cipriani, V. Di Dio, F. Genduso, D. La Cascia, R. Liga, R. Miceli, G.R. Galluzzo, Perspective on hydrogen energy carrier and its automotive applications, *Int. J. Hydrogen Energy*. 39 (2014) 8482–8494, <https://doi.org/10.1016/j.ijhydene.2014.03.174>.
- [7] F. Jiao, B. Xu, Electrochemical ammonia synthesis and ammonia fuel cells, *Adv. Mater.* 31 (31) (2019) 1805173.
- [8] J. Ikäheimo, J. Kiviluoma, R. Weiss, H. Holttinen, Power-to-ammonia in future North European 100 % renewable power and heat system, *Int. J. Hydrogen Energy*. 43 (2018) 17295–17308, <https://doi.org/10.1016/j.ijhydene.2018.06.121>.
- [9] J.M. Ogden, Prospects for building a hydrogen energy infrastructure, *Annu. Rev. Energy Environ.* 24 (1999) 227–279, <https://doi.org/10.1146/annurev.energy.24.1.227>.
- [10] D.R. MacFarlane, P.V. Cherepanov, J. Choi, B.H.R. Suryanto, R.Y. Hodgetts, J. M. Bakker, F.M.F. Vallana, A.N. Simonov, A roadmap to the ammonia economy, *Joule*. 4 (2020) 1186–1205, <https://doi.org/10.1016/j.joule.2020.04.004>.
- [11] C.H. Christensen, T. Johannessen, R.Z. Sørensen, J.K. Nørskov, Towards an ammonia-mediated hydrogen economy? *Catal. Today*. 111 (2006) 140–144, <https://doi.org/10.1016/j.cattod.2005.10.011>.
- [12] J.W. Erisman, M.A. Sutton, J. Galloway, Z. Klimont, W. Winiwarter, How a century of ammonia synthesis changed the world, *Nat. Geosci.* 1 (2008) 636–639, <https://doi.org/10.1038/ngeo325>.
- [13] N. Morlanés, S.P. Katikaneni, S.N. Paglieri, A. Harale, B. Solami, S.M. Sarathy, J. Gascon, A technological roadmap to the ammonia energy economy: current state and missing technologies, *Chem. Eng. J.* 408 (2021), 127310, <https://doi.org/10.1016/j.cej.2020.127310>.

- [14] W.S. Chai, Y. Bao, P. Jin, G. Tang, L. Zhou, A review on ammonia, ammonia-hydrogen and ammonia-methane fuels, *Renew. Sustain. Energy Rev.* 147 (2021), 111254, <https://doi.org/10.1016/j.rser.2021.111254>.
- [15] P. Glarborg, J.A. Miller, B. Ruscic, S.J. Klippenstein, Modeling nitrogen chemistry in combustion, *Prog. Energy Combust. Sci.* 67 (2018) 31–68, <https://doi.org/10.1016/j.pecs.2018.01.002>.
- [16] M. Abian, M.U. Alzueta, P. Glarborg, Formation of NO from N₂/O₂ mixtures in a flow reactor: Toward an accurate prediction of thermal NO, *Int. J. Chem. Kinet.* 47 (2015) 518–532, <https://doi.org/10.1002/kin.20929>.
- [17] P. Forster, V. Ramaswamy, P. Artaxo, T. Bernsten, R. Betts, D.W. Fahey, J. Haywood, J. Lean, D.C. Lowe, G. Myhre, et al., *Phys. Sci. Basis*, 2007, p. 2007.
- [18] S.J. Klippenstein, L.B. Harding, P. Glarborg, J.A. Miller, The role of NNH in NO formation and control, *Combust. Flame.* 158 (2011) 774–789, <https://doi.org/10.1016/j.combustflame.2010.12.013>.
- [19] S.J. Klippenstein, M. Pfeifle, A.W. Jasper, P. Glarborg, Theory and modeling of relevance to prompt-NO formation at high pressure, *Combust. Flame.* 195 (2018) 3–17, <https://doi.org/10.1016/j.combustflame.2018.04.029>.
- [20] A. Stagni, C. Cavallotti, S. Arunthanayothin, Y. Song, O. Herbinet, F. Battin-Leclerc, T. Faravelli, An experimental, theoretical and kinetic-modeling study of the gas-phase oxidation of ammonia, *React. Chem. Eng.* 5 (2020) 696–711, <https://doi.org/10.1039/c9re00429g>.
- [21] S.J. Klippenstein, From theoretical reaction dynamics to chemical modeling of combustion, *Proc. Combust. Inst.* 36 (2017) 77–111, <https://doi.org/10.1016/j.proci.2016.07.100>.
- [22] C. Cavallotti, M. Pelucchi, Y. Georgievskii, S.J. Klippenstein, EStokTP: electronic structure to temperature- and pressure-dependent rate constants—a code for automatically predicting the thermal kinetics of reactions, *J. Chem. Theory Comput.* 15 (2019) 1122–1145, <https://doi.org/10.1021/acs.jctc.8b00701>.
- [23] A. Klerke, C.H. Christensen, J.K. Norskov, T. Vegge, Ammonia for hydrogen storage: challenges and opportunities, *J. Mater. Chem.* 18 (2008) 2304–2310, <https://doi.org/10.1039/B720020J>.
- [24] C. Zamfirescu, I. Dincer, Ammonia as a green fuel and hydrogen source for vehicular applications, *Fuel Process. Technol.* 90 (2009) 729–737, <https://doi.org/10.1016/j.fuproc.2009.02.004>.
- [25] C.S. Mørch, A. Bjerre, M.P. Gøttrup, S.C. Sorenson, J. Schramm, Ammonia/hydrogen mixtures in an SI-engine: engine performance and analysis of a proposed fuel system, *Fuel.* 90 (2011) 854–864, <https://doi.org/10.1016/j.fuel.2010.09.042>.
- [26] S. Frigo, R. Gentili, Analysis of the behaviour of a 4-stroke Si engine fuelled with ammonia and hydrogen, *Int. J. Hydrogen Energy.* 38 (2013) 1607–1615, <https://doi.org/10.1016/j.ijhydene.2012.10.114>.
- [27] M. Comotti, S. Frigo, Hydrogen generation system for ammonia–hydrogen fuelled internal combustion engines, *Int. J. Hydrogen Energy.* 40 (2015) 10673–10686, <https://doi.org/10.1016/j.ijhydene.2015.06.080>.
- [28] C. Lhuillier, P. Brequigny, F. Contino, C. Mounaim-Rousselle, Experimental study on ammonia/hydrogen/air combustion in spark ignition engine conditions, *Fuel.* 269 (2020), 117448, <https://doi.org/10.1016/j.fuel.2020.117448>.
- [29] A. Valera-Medina, D.G. Pugh, P. Marsh, G. Bulat, P. Bowen, Preliminary study on lean premixed combustion of ammonia-hydrogen for swirling gas turbine combustors, *Int. J. Hydrogen Energy.* 42 (2017) 24495–24503, <https://doi.org/10.1016/j.ijhydene.2017.08.028>.
- [30] A. Valera-Medina, M. Gutesa, H. Xiao, D. Pugh, A. Giles, B. Goktepe, R. Marsh, P. Bowen, Premixed ammonia/hydrogen swirl combustion under rich fuel conditions for gas turbines operation, *Int. J. Hydrogen Energy.* 44 (2019) 8615–8626, <https://doi.org/10.1016/j.ijhydene.2019.02.041>.
- [31] J.A. Wünnig, J.G. Wünnig, Flameless oxidation to reduce thermal no-formation, *Prog. Energy Combust. Sci.* 23 (1997) 81–94, [https://doi.org/10.1016/s0360-1285\(97\)00006-3](https://doi.org/10.1016/s0360-1285(97)00006-3).
- [32] A. Stagni, A. Frassoldati, M. Pelucchi, T. Faravelli, Chemistry of nitrogen oxides (NOx) formation in flameless combustion, in: *Fundam. Low Emiss. Flameless Combust. Its Appl.*, Elsevier, 2022: pp. 421–451. <https://doi.org/10.1016/b978-0-323-85244-9.00011-3>.
- [33] A. Cavaliere, M. De Joannon, Mild combustion, *Prog. Energy Combust. Sci.* 30 (2004) 329–366, <https://doi.org/10.1016/j.pecs.2004.02.003>.
- [34] A. Kéromnès, W.K. Metcalfe, K.A. Heufer, N. Donohoe, A.K. Das, C.-J. Sung, J. Herzler, C. Naumann, P. Griebel, O. Mathieu, M.C. Krejci, E.L. Petersen, W. J. Pitz, H.J. Curran, An experimental and detailed chemical kinetic modeling study of hydrogen and syngas mixture oxidation at elevated pressures, *Combust. Flame.* 160 (6) (2013) 995–1011.
- [35] W.K. Metcalfe, S.M. Burke, S.S. Ahmed, H.J. Curran, A hierarchical and comparative kinetic modeling study of C1–C2 hydrocarbon and oxygenated fuels, *Int. J. Chem. Kinet.* 45 (2013) 638–675, <https://doi.org/10.1002/kin.20802>.
- [36] P.D. Ronney, Effect of chemistry and transport properties on near-limit flames at microgravity, *Combust. Sci. Technol.* 59 (1988) 123–141, <https://doi.org/10.1080/00102208808947092>.
- [37] Y. Song, H. Hashemi, J.M. Christensen, C. Zou, P. Marshall, P. Glarborg, Ammonia oxidation at high pressure and intermediate temperatures, *Fuel.* 181 (2016) 358–365, <https://doi.org/10.1016/j.fuel.2016.04.100>.
- [38] O. Mathieu, E.L. Petersen, Experimental and modeling study on the high-temperature oxidation of ammonia and related NOx chemistry, *Combust. Flame.* 162 (2015) 554–570, <https://doi.org/10.1016/j.combustflame.2014.08.022>.
- [39] P. Dagaut, On the oxidation of ammonia and mutual sensitization of the oxidation of no and ammonia: experimental and kinetic modeling, *Combust. Sci. Technol.* 194 (2022) 117–129, <https://doi.org/10.1080/00102202.2019.1678380>.
- [40] M. Benés, G. Pozo, M. Abián, Á. Millera, R. Bilbao, M.U. Alzueta, Experimental study of the pyrolysis of NH₃ under flow reactor conditions, *Energy Fuels.* 35 (2021) 7193–7200, <https://doi.org/10.1021/acs.energyfuels.0c03387>.
- [41] M. Abián, M. Benés, A. de Goñi, B. Muñoz, M.U. Alzueta, Study of the oxidation of ammonia in a flow reactor. Experiments and kinetic modeling simulation, *Fuel.* 300 (2021), 120979, <https://doi.org/10.1016/j.fuel.2021.120979>.
- [42] S.A. Alturaifi, O. Mathieu, E.L. Petersen, An experimental and modeling study of ammonia pyrolysis, *Combust. Flame.* 235 (2022), 111694, <https://doi.org/10.1016/j.combustflame.2021.111694>.
- [43] J. Chen, X. Jiang, X. Qin, Z. Huang, Effect of hydrogen blending on the high temperature auto-ignition of ammonia at elevated pressure, *Fuel.* 287 (2021), 119563, <https://doi.org/10.1016/j.fuel.2020.119563>.
- [44] S.A. Alturaifi, O. Mathieu, E.L. Petersen, A shock-tube study of NH₃ and NH₃/H₂ oxidation using laser absorption of NH₃ and H₂O, *Proc. Combust. Inst.* 39 (1) (2023) 233–241.
- [45] M. Pochet, V. Dias, B. Moreau, F. Foucher, H. Jeanmart, F. Contino, Experimental and numerical study, under LTC conditions, of ammonia ignition delay with and without hydrogen addition, *Proc. Combust. Inst.* 37 (2019) 621–629, <https://doi.org/10.1016/j.proci.2018.05.138>.
- [46] L. Dai, S. Gersen, P. Glarborg, H. Levinsky, A. Mokhov, Experimental and numerical analysis of the autoignition behavior of NH₃ and NH₃/H₂ mixtures at high pressure, *Combust. Flame.* 215 (2020) 134–144, <https://doi.org/10.1016/j.combustflame.2020.01.023>.
- [47] X. He, B. Shu, D. Nascimento, K. Moshhammer, M. Costa, R.X. Fernandes, Auto-ignition kinetics of ammonia and ammonia/hydrogen mixtures at intermediate temperatures and high pressures, *Combust. Flame.* 206 (2019) 189–200.
- [48] P. Sabia, M.V. Manna, R. Ragucci, M. de Joannon, Mutual inhibition effect of hydrogen and ammonia in oxidation processes and the role of ammonia as “strong” collider in third-molecular reactions, *Int. J. Hydrogen Energy.* 45 (2020) 32113–32127, <https://doi.org/10.1016/j.ijhydene.2020.08.218>.
- [49] X. Zhang, S.P. Moosakutty, R.P. Rajan, M. Younes, S.M. Sarathy, Combustion chemistry of ammonia/hydrogen mixtures: Jet-stirred reactor measurements and comprehensive kinetic modeling, *Combust. Flame.* 234 (2021), 111653, <https://doi.org/10.1016/j.combustflame.2021.111653>.
- [50] M.V. Manna, P. Sabia, G. Sorrentino, T. Viola, R. Ragucci, M. de Joannon, New insight into NH₃-H₂ mutual inhibiting effects and dynamic regimes at low-intermediate temperatures, *Combust. Flame.* 243 (2022), 111957, <https://doi.org/10.1016/j.combustflame.2021.111957>.
- [51] A. Stagni, Y. Song, L.A. Vandewalle, K.M. Van Geem, G.B. Marin, O. Herbinet, F. Battin-Leclerc, T. Faravelli, The role of chemistry in the oscillating combustion of hydrocarbons: an experimental and theoretical study, *Chem. Eng. J.* 385 (2019), 123401, <https://doi.org/10.1016/j.cej.2019.123401>.
- [52] J.H. Lee, J.H. Kim, J.H. Park, O.C. Kwon, Studies on properties of laminar premixed hydrogen-added ammonia/air flames for hydrogen production, *Int. J. Hydrogen Energy.* 35 (2010) 1054–1064, <https://doi.org/10.1016/j.ijhydene.2009.11.071>.
- [53] A. Ichikawa, A. Hayakawa, Y. Kitagawa, K.D. Kunkuma Amila Somarathne, T. Kudo, H. Kobayashi, Laminar burning velocity and markstein length of ammonia/hydrogen/air premixed flames at elevated pressures, *Int. J. Hydrogen Energy.* 40 (30) (2015) 9570–9578.
- [54] J. Li, H. Huang, N. Kobayashi, Z. He, Y. Osaka, T. Zeng, Numerical study on effect of oxygen content in combustion air on ammonia combustion, *Energy.* 93 (2015) 2053–2068, <https://doi.org/10.1016/j.energy.2015.10.060>.
- [55] P. Kumar, T.R. Meyer, Experimental and modeling study of chemical-kinetics mechanisms for H₂-NH₃-air mixtures in laminar premixed jet flames, *Fuel.* 108 (2013) 166–176, <https://doi.org/10.1016/j.fuel.2012.06.103>.
- [56] X. Han, Z. Wang, M. Costa, Z. Sun, Y. He, K. Cen, Experimental and kinetic modeling study of laminar burning velocities of NH₃/air, NH₃/H₂/air, NH₃/CO/air and NH₃/CH₄/air premixed flames, *Combust. Flame.* 206 (2019) 214–226.
- [57] C. Lhuillier, P. Brequigny, N. Lamoureux, F. Contino, C. Mounaim-Rousselle, Experimental investigation on laminar burning velocities of ammonia/hydrogen/air mixtures at elevated temperatures, *Fuel.* 263 (2020), 116653, <https://doi.org/10.1016/j.fuel.2019.116653>.
- [58] K.P. Shrestha, C. Lhuillier, A.A. Barbosa, P. Brequigny, F. Contino, C. Mounaim-Rousselle, L. Seidel, F. Mauss, An experimental and modeling study of ammonia with enriched oxygen content and ammonia/hydrogen laminar flame speed at elevated pressure and temperature, *Proc. Combust. Inst.* 38 (2021) 2163–2174, <https://doi.org/10.1016/j.proci.2020.06.197>.
- [59] A. Stagni, C. Cavallotti, H-abstractions by O₂, NO₂, NH₂, and HO₂ from H₂NO: Theoretical study and implications for ammonia low-temperature kinetics, *Proc. Combust. Inst.* 39 (1) (2023) 633–641.
- [60] S.J. Klippenstein, P. Glarborg, Theoretical kinetics predictions for NH₂ + HO₂, *Combust. Flame.* 236 (2022), 111787, <https://doi.org/10.1016/j.combustflame.2021.111787>.
- [61] K.P. Shrestha, L. Seidel, T. Zeuch, F. Mauss, Detailed Kinetic Mechanism for the Oxidation of Ammonia Including the Formation and Reduction of Nitrogen Oxides, *Energy and Fuels.* 32 (2018) 10202–10217, <https://doi.org/10.1021/acs.energyfuels.8b01056>.
- [62] J. Otomo, M. Koshi, T. Mitsumori, H. Iwasaki, K. Yamada, Chemical kinetic modeling of ammonia oxidation with improved reaction mechanism for ammonia/air and ammonia/hydrogen/air combustion, *Int. J. Hydrogen Energy.* 43 (2018) 3004–3014, <https://doi.org/10.1016/j.ijhydene.2017.12.066>.
- [63] E.C. Okafor, Y. Naito, S. Colson, A. Ichikawa, T. Kudo, A. Hayakawa, H. Kobayashi, Experimental and numerical study of the laminar burning velocity of CH₄-NH₃-air premixed flames, *Combust. Flame.* 187 (2018) 185–198, <https://doi.org/10.1016/j.combustflame.2017.09.002>.

- [64] S. Arunthanayothin, A. Stagni, Y.u. Song, O. Herbinet, T. Faravelli, F. Battin-Leclerc, Ammonia-methane interaction in jet-stirred and flow reactors: An experimental and kinetic modeling study, *Proc. Combust. Inst.* 38 (1) (2021) 345–353.
- [65] Y. Song, L. Marrodán, N. Vin, O. Herbinet, E. Assaf, C. Fittschen, A. Stagni, T. Faravelli, M.U.U. Alzueta, F. Battin-Leclerc, The sensitizing effects of NO₂ and NO on methane low temperature oxidation in a jet stirred reactor, *Proc. Combust. Inst.* 37 (2019) 667–675, <https://doi.org/10.1016/j.proci.2018.06.115>.
- [66] Y. Li, S.M. Sarathy, Probing hydrogen–nitrogen chemistry: A theoretical study of important reactions in N_xH_y, HCN and HNC₂ oxidation, *Int. J. Hydrogen Energy*. 45 (2020) 23624–23637, <https://doi.org/10.1016/j.ijhydene.2020.06.083>.
- [67] S.J. Klippenstein, L.B. Harding, B. Ruscic, R. Sivaramakrishnan, N.K. Srinivasan, M. C. Su, J.V. Michael, Thermal decomposition of NH₂OH and subsequent reactions: Ab initio transition state theory and reflected shock tube experiments, *J. Phys. Chem. A*. 113 (2009) 10241–10259, <https://doi.org/10.1021/jp905454k>.
- [68] D.L. Baulch, C.T. Bowman, C.J. Cobos, R.A. Cox, T.h. Just, J.A. Kerr, M.J. Pilling, D. Stocker, J. Troe, W. Tsang, R.W. Walker, J. Warnatz, Others, Evaluated kinetic data for combustion modeling: supplement II, *J. Phys. Chem. Ref. Data*. 34 (3) (2005) 757–1397.
- [69] C.J. Howard, Kinetic study of the equilibrium HO₂ + NO ⇌ OH + NO₂ and the thermochemistry of HO₂, *J. Am. Chem. Soc.* 102 (1980) 6937–6941, <https://doi.org/10.1021/ja00543a006>.
- [70] S. Song, R.K. Hanson, C.T. Bowman, D.M. Golden, A shock tube study of the product branching ratio of the NH₂ + NO reaction at high temperatures, *J. Phys. Chem. A*. 106 (2002) 9233–9235, <https://doi.org/10.1021/jp020943d>.
- [71] P. Glarborg, P.G. Kristensen, K. Dam-Johansen, M.U. Alzueta, A. Millera, R. Bilbao, Nitric oxide reduction by non-hydrocarbon fuels, Implications for reburning with gasification gases, *Energy Fuels*. 14 (2000) 828–838, <https://doi.org/10.1021/ef990186r>.
- [72] A.M. Dean, J.W. Bozzelli, Combustion Chemistry of Nitrogen, in: *Gas-Phase Combust. Chem.*, 2000: pp. 125–341. https://doi.org/10.1007/978-1-4612-1310-9_2.
- [73] R. Sumathi, D. Sengupta, M.T. Nguyen, Theoretical study of the H₂ + NO and related reactions of [H₂NO] isomers, *J. Phys. Chem. A*. 102 (1998) 3175–3183, <https://doi.org/10.1021/jp9804953>.
- [74] P. Glarborg, H. Hashemi, S. Cheski, A.W. Jasper, On the Rate Constant for NH₂+HO₂ and Third-Body Collision Efficiencies for NH₂+H (+M) and NH₂+NH₂ (+M), *J. Phys. Chem. A*. 125 (2021) 1505–1516, <https://doi.org/10.1021/acs.jpca.0c11011>.
- [75] D.F. Davidson, K. Kohse-Höinghaus, A.Y. Chang, R.K. Hanson, A pyrolysis mechanism for ammonia, *Int. J. Chem. Kinet.* 22 (1990) 513–535, <https://doi.org/10.1002/kin.550220508>.
- [76] P.L. Mar, K.S. Werpetinski, M. Cook, A study of the reaction H + O₂ = HO₂ = O + OH at four levels of density-functional theory, *Chem. Phys. Lett.* 287 (1998) 195–201, [https://doi.org/10.1016/S0009-2614\(98\)00158-4](https://doi.org/10.1016/S0009-2614(98)00158-4).
- [77] Z. Hong, D.F. Davidson, E.A. Barbour, R.K. Hanson, A new shock tube study of the H + O₂ → OH + O reaction rate using tunable diode laser absorption of H₂O near 2.5 μm, *Proc. Combust. Inst.* 33 (2011) 309–316, <https://doi.org/10.1016/j.proci.2010.05.101>.
- [78] J.W. Sutherland, J.V. Michael, A.N. Pirraglia, F.L. Nesbitt, R.B. Klemm, Rate constant for the reaction of O(3P) with H₂ by the flash photolysis-shock tube and flash photolysis-resonance fluorescence techniques; 504K ≤ T ≤ 2495K, *Symp. Combust.*, in, 1988, pp. 929–941.
- [79] L.T. Zaczek, K.Y. Lam, D.F. Davidson, R.K. Hanson, A shock tube study of CH₃OH + OH → products using OH laser absorption, *Proc. Combust. Inst.* 35 (2015) 377–384, <https://doi.org/10.1016/j.proci.2014.05.051>.
- [80] J. Li, Z. Zhao, A. Kazakov, F.L. Dryer, An updated comprehensive kinetic model of hydrogen combustion, *Int. J. Chem. Kinet.* 36 (2004) 566–575, <https://doi.org/10.1002/kin.20026>.
- [81] A. Cuoci, A. Frassoldati, T. Faravelli, E. Ranzi, OpenSMOKE++: An object-oriented framework for the numerical modeling of reactive systems with detailed kinetic mechanisms, *Comput. Phys. Commun.* 192 (2015) 237–264, <https://doi.org/10.1016/j.cpc.2015.02.014>.
- [82] O. Herbinet, G. Dayma, *Jet-stirred reactors*, *Clean. Combust.*, Springer, in, 2013, pp. 183–210.
- [83] H. Nakamura, M. Shindo, Effects of radiation heat loss on laminar premixed ammonia/air flames, *Proc. Combust. Inst.* 37 (2019) 1741–1748, <https://doi.org/10.1016/j.proci.2018.06.138>.
- [84] M.F. Modest, *Radiative Heat Transfer: Second Edition*, 2003. <https://doi.org/10.1016/B978-0-12-503163-9.X5000-0>.
- [85] B. Mei, J. Zhang, X. Shi, Z. Xi, Y. Li, Enhancement of ammonia combustion with partial fuel cracking strategy: Laminar flame propagation and kinetic modeling investigation of NH₃/H₂/N₂/air mixtures up to 10 atm, *Combust. Flame*. 231 (2021), 111472, <https://doi.org/10.1016/j.combustflame.2021.111472>.
- [86] Y.B. Zel'dovich, The oxidation of nitrogen in combustion explosions, *Acta Physicochim. U.S.S.R.* 21 (1946) 577–628.
- [87] J.D. Adamson, S.K. Farhat, C.L. Morter, G.P. Glass, R.F. Curl, L.F. Phillips, The reaction of NH₂ with O, *J. Phys. Chem.* 98 (1994) 5665–5669, <https://doi.org/10.1021/j100073a016>.
- [88] P. Dransfeld, W. Hack, H. Kurzke, F. Temps, H.G. Wagner, Direct studies of elementary reactions of NH₂-radicals in the gas phase, *Symp. Combust.*, in, 1985, pp. 655–663.
- [89] J.W. Bozzelli, A.M. Dean, Energized complex quantum rice-ramsparger-kassel analysis on reactions of amidogen with hydroperoxy, oxygen and oxygen atoms, *J. Phys. Chem.* 93 (1989) 1058–1065, <https://doi.org/10.1021/j100340a009>.
- [90] S.H. Mousavipour, F. Pirhadi, A. Habibagahi, A theoretical investigation on the kinetics and mechanism of the reaction of amidogen with hydroxyl radical, *J. Phys. Chem. A*. 113 (2009) 12961–12971, <https://doi.org/10.1021/jp905197h>.
- [91] A. Kéromnès, *Rapid compression machines*, *Green Energy Technol.*, Springer, in, 2013, pp. 163–181.
- [92] R.K. Lyon, Thermal DeNO_x Controlling nitrogen oxides emissions by a noncatalytic process, *Environ. Sci. Technol.* 21 (1987) 231–236, <https://doi.org/10.1021/es00157a002>.
- [93] H. Xiao, H. Li, Experimental and kinetic modeling study of the laminar burning velocity of NH₃/DME/air premixed flames, *Combust. Flame*. 245 (2022) 1–13, <https://doi.org/10.1016/j.combustflame.2022.112372>.